DESIGN AND ANALYSIS OF A VERTICAL AXIS WATER TURBINE FOR RIVER APPLICATIONS USING COMPUTATIONAL FLUID DYNAMICS

A THESIS SUBMITTED TO
THE GRADUATE SCHOOL OF NATURAL AND APPLIED SCIENCES
OF
MIDDLE EAST TECHNICAL UNIVERSITY

BY

EREN DEMİRCAN

IN PARTIAL FULFILLMENT OF THE REQUIREMENTS
FOR
THE DEGREE OF MASTER OF SCIENCE
IN
MECHANICAL ENGINEERING

JANUARY 2014

Approval of the thesis:

DESIGN AND ANALYSIS OF A VERTICAL AXIS WATER TURBINE FOR RIVER APPLICATIONS USING COMPUTATIONAL FLUID DYNAMICS

submitted by **EREN DEMİRCAN** in partial fulfillment of the requirements for the degree of **Master of Science in Mechanical Engineering Department, Middle East Technical University** by,

Prof. Dr. Canan Özgen _____
Dean, Graduate School of **Natural and Applied Sciences**

Prof. Dr. Süha Oral _____
Head of Department, **Mechanical Engineering**

Prof. Dr. M. Haluk Aksel _____
Supervisor, **Mechanical Engineering Dept., METU**

Assist. Prof. Dr. M. Metin Yavuz _____
Co-supervisor, **Mechanical Engineering Dept., METU**

Examining Committee Members:

Prof. Dr. Kahraman ALBAYRAK
Mechanical Engineering Dept., METU _____

Prof. Dr. M. Haluk AKSEL
Mechanical Engineering Dept., METU _____

Assist. Prof. Dr. M. Metin YAVUZ
Mechanical Engineering Dept., METU _____

Dr. Tahsin ÇETİNKAYA
Mechanical Engineering Dept., METU _____

Assoc. Prof. Dr. Oğuz UZOL
Aerospace Engineering Dept., METU _____

Date: **24.01.2014**

I hereby declare that all information in this document has been obtained and presented in accordance with academic rules and ethical conduct. I also declare that, as required by these rules and conduct, I have fully cited and referenced all material and results that are not original to this work.

Name, Last Name: EREN DEMİRCAN

Signature :

ABSTRACT

DESIGN AND ANALYSIS OF A VERTICAL AXIS WATER TURBINE FOR RIVER APPLICATIONS USING COMPUTATIONAL FLUID DYNAMICS

Demircan, Eren
M.S., Department of Mechanical Engineering
Supervisor : Prof. Dr. M. Haluk Aksel
Co-Supervisor : Assist. Prof. Dr. M. Metin Yavuz

January 2014, 57 pages

The main purpose of this study is to design a Darrieus rotor type vertical axis water turbine using Computational Fluid Dynamics (CFD) in order to be used in river currents. The CFD modeling is based on two dimensional numerical solution of the rotor motion using commercial Unsteady Reynolds Averaged Navier-Stokes solvers, Ansys Fluent and CFX. To validate the two dimensional numerical solution, an experimental Darrieus rotor type water turbine from literature is studied and performance of several turbulence models are examined. A Darrieus rotor type vertical axis water turbine is designed for low speed water currents using QBlade which is an open source sofware used to calculate the performance of the vertical axis turbines. Two dimensional numerical modeling of the designed turbine is performed and results are compared with QBlade results.

Keywords: Vertical axis water turbine, Darrieus rotor type, Computational Fluid Dynamics

ÖZ

HESAPLAMALI AKIŞKANLAR DİNAMİĞİ KULLANILARAK NEHİR UYGULAMALARI İÇİN DİKEY EKSENLİ SU TÜRBİNİ TASARIMI VE ANALİZİ

Demircan, Eren
Yüksek Lisans, Makina Mühendisliği Bölümü
Tez Yöneticisi : Prof. Dr. M. Haluk Aksel
Ortak Tez Yöneticisi : Yrd. Doç. Dr. M. Metin Yavuz

Ocak 2014 , 57 sayfa

Bu çalışmanın temel amacı, Hesaplamalı Akışkanlar Dinamiği (HAD) yardımıyla nehir akımlarında kullanılmak üzere bir Darrieus rotor tipi dikey eksenli su türbini tasarlanmasıdır. HAD modellemesi ticari Reynolds-ortalamalı Navier-Stokes çözücüleri olan Ansys Fluent ve CFX kullanılarak rotor hareketinin iki boyutlu sayısal çözümüne dayanmaktadır. İki boyutlu sayısal çözümü doğrulamak için, literatürden deneysel bir Darrieus rotor tipi dikey eksenli su türbini çalışılmış ve çeşitli türbülans modellerinin performansı incelenmiştir. Dikey eksenli türbinlerin performansını hesaplamak için kullanılan QBlade açık kaynaklı yazılımı ile düşük hızlı su akımları için Darrieus rotor tipi dikey eksenli bir su türbini tasarlanmıştır. Tasarlanan türbinin iki boyutlu sayısal modellenmesi gerçekleştirilmiş ve sonuçlar QBlade sonuçları ile karşılaştırılmıştır.

Anahtar Kelimeler: Dikey eksenli su türbini, Darrieus rotor tipi, Hesaplamalı Akışkanlar Dinamiği

to my family and woman of my life ...

ACKNOWLEDGMENTS

I would like to express my gratitude to my supervisor Prof. Dr. M. Haluk Aksel and co-supervisor Assist. Prof. Dr. M. Metin Yavuz for their guidance, criticism and support throughout this work.

I would also like to express my appreciation to my examining committee members Prof. Dr. Kahraman Albayrak, Dr. Tahsin Çetinkaya and Assoc. Prof. Dr. Oğuz Uzol for their valuable suggestions and comments.

I am thankful to my friends and workmates Osman Akdağ, Alper Çelik and Ali Karakuş for their technical and moral support all throughout this study.

Especially, I owe my sincere gratitude to my parents Hüsnüye and Aliekber Demircan and my sister Ezgi Demircan for their support all through my life.

I am grateful to my love, Zeynep Eliş Demircan, for her encouragement, understanding and patience. It would be impossible to finish this work without her.

TABLE OF CONTENTS

LIST OF TABLES

TABLES

LIST OF FIGURES

FIGURES

LIST OF ABBREVIATIONS

A_{ref}	Reference Swept Area of Turbine
c	Chord Length of Blade
C_P	Power Coefficient of Turbine
C_T	Torque Coefficient of Turbine
C_f	Skin Friction Coefficient
F^*	Reduced Frequency
H	Height of Turbine
N	Number of Blades
P	Power Produced by Turbine
R	Radius of Turbine
Re_c	Chord Reynolds Number
T	Torque Produced by Turbine
u_*	Friction Velocity
V_0	Free Stream Velocity
V_R	Relative Velocity
V_θ	Tangential Velocity
y	Node Distance to Wall
y^+	Non-dimensional Value for Relative Distance of the First Node from Wall Surface
α	Angle of Attack
α_{max}	Maximum Angle of Attack
θ	Azimuthal Angle
ω	Rotational Velocity
λ	Tip Speed Ratio
σ	Solidity Ratio
ρ	Density
μ	Dynamic Viscosity
τ_w	Wall Shear Stress
Δt	Time Step

CHAPTER 1

INTRODUCTION

In recent years, renewable energy sources draw attention due to reduction of fossil fuels and increasing energy demand of the world. In addition, renewable energy sources are becoming popular because of global warming and environmental concerns. Many investigations have been made in renewable energy field such as wind, solar, ocean wave and tidal current energy. Tidal current energy is also a promising energy source especially for oceanfront countries. Canada, for example, can meet 63 % of its energy demand from available tidal power around [1]. UK can also generate 40 % of its electricity demand from tidal power if tidal and wave sources were employed effectively [2].

Tidal energy is converted into useful power by using tidal stream turbines. They are also called as low head turbines, hydrokinetic turbines or water turbines. Although they are less efficient than commercial water turbines used in hydroelectric power stations, these turbines do not need construction of a dam or waterway. Hydrokinetic turbines harness the kinetic energy of tidal or river stream and convert to useful power. These turbines are like commercial wind turbines operating in water stream. Their classification and technology are similar with wind turbines. They are classified by their axis of rotation as horizontal axis water turbines (HAWT) and vertical axis water turbines (VAWT). A horizontal axis water turbine and a vertical axis water turbine can be seen in Figure 1.1. HAWTs need pitch control mechanism since they generate power in one or two way flow. On the other hand, VAWTs do not need pitch control mechanism and they can operate regardless of flow direction [3]. However, VAWTs are less efficient than HAWTs.

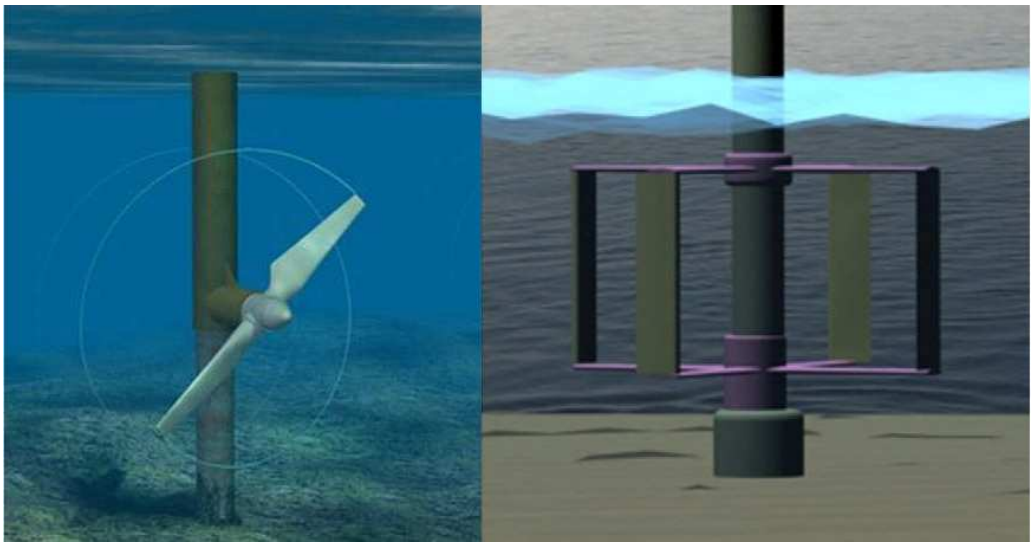

Figure 1.1: Horizontal and Vertical Axis Water Turbines [3]

Vertical axis turbines are simply categorized by their rotor type. Savonious and Darrieus rotor type turbines are the most well known ones and they are shown in Figure 1.2. Savonius rotor type turbine operates with the drag force created by the flow whereas Darrieus rotor type turbine is driven by the force induced by the lift and drag forces.

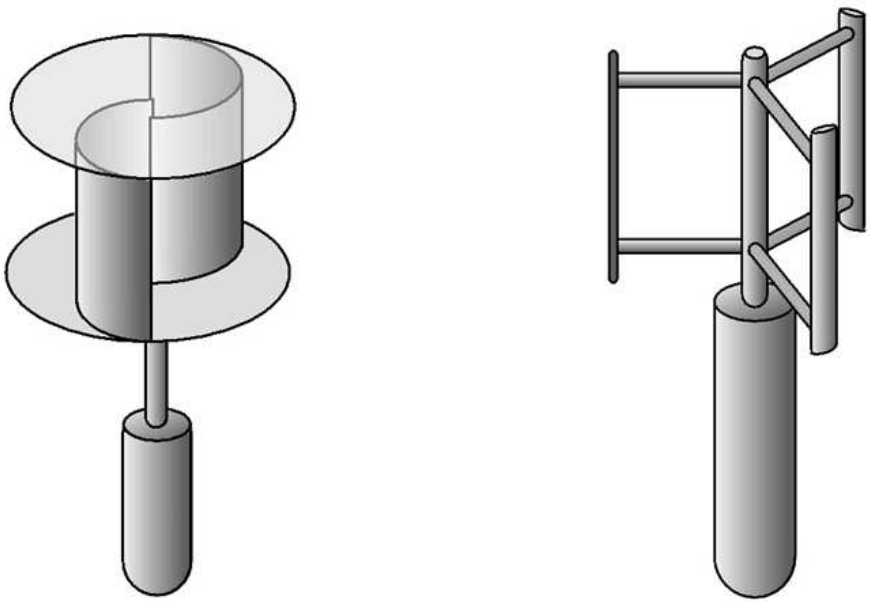

Figure 1.2: Savonious and Darrieus Rotor Type Turbines [4]

Over the past few decades, the usage of straight bladed Darrieus water turbines has become popular in harnessing tidal power [4]. The main drawbacks are lower efficiency compared to horizontal axis turbines and the variation in the torque generated. On the other hand, the main advantages of Darrieus turbines are their geometric simplicity and compactness. Furthermore, the power density per square meter could be higher than the configurations used before. In other words, Darrieus turbines can be used closer to each other than horizontal axis turbines [5].

1.1 Flow Dynamics of Darrieus Turbine

The power extracted from the flow of any medium by a hydrokinetic turbine is proportional to the kinetic energy passing per unit time and given by

$$P = C_P \frac{1}{2} \rho A_{ref} V_0^3 \tag{1.1}$$

where C_P is the power coefficient of the turbine, ρ is the density of working fluid, V_0 is the free stream velocity and A_{ref} is turbine swept area normal to the direction of flow. For vertical axis turbine A_{ref} is defined as

$$A_{ref} = 2RH \tag{1.2}$$

where R and H are being the radius and height of the turbine, respectively [6].

Straight bladed Darrieus turbine is the simplest type of vertical axis turbines that are used both in wind and water flow. A simple straight bladed Darrieus turbine is shown Figure 1.3. Although the geometry of straight bladed Darrieus turbine is simple, flow field across the turbine is extremely unsteady and largely three dimensional. Understanding of complex flow structures in Darrieus turbine is significant in order to increase the turbine performance. In Figure 1.4, velocity triangles of a Darrieus turbine blade are shown at different azimuth angle positions θ. As the turbine rotates, a resultant velocity is encountered due to the appropriate combination of V_0 and the tangential velocity $V_\theta = \omega R$. The relative velocity for the blade at any azimuthal position is expressed by,

$$V_R = \sqrt{(V_0 + V_\theta \cos\theta)^2 + (V_\theta \sin\theta)^2} \tag{1.3}$$

where V_0 is the free stream velocity and V_θ is the tangential velocity [7].

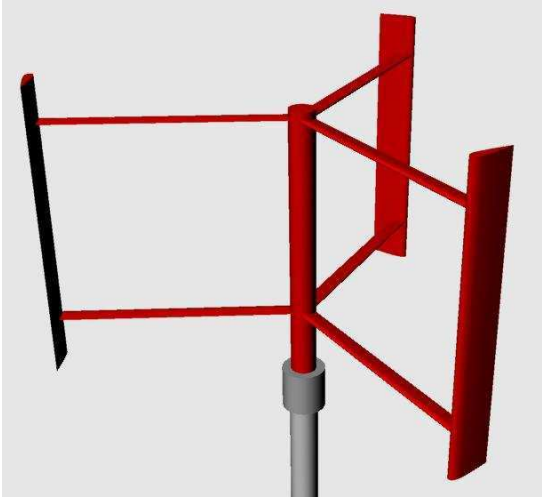

Figure 1.3: Straight Bladed Darrieus Turbine [6]

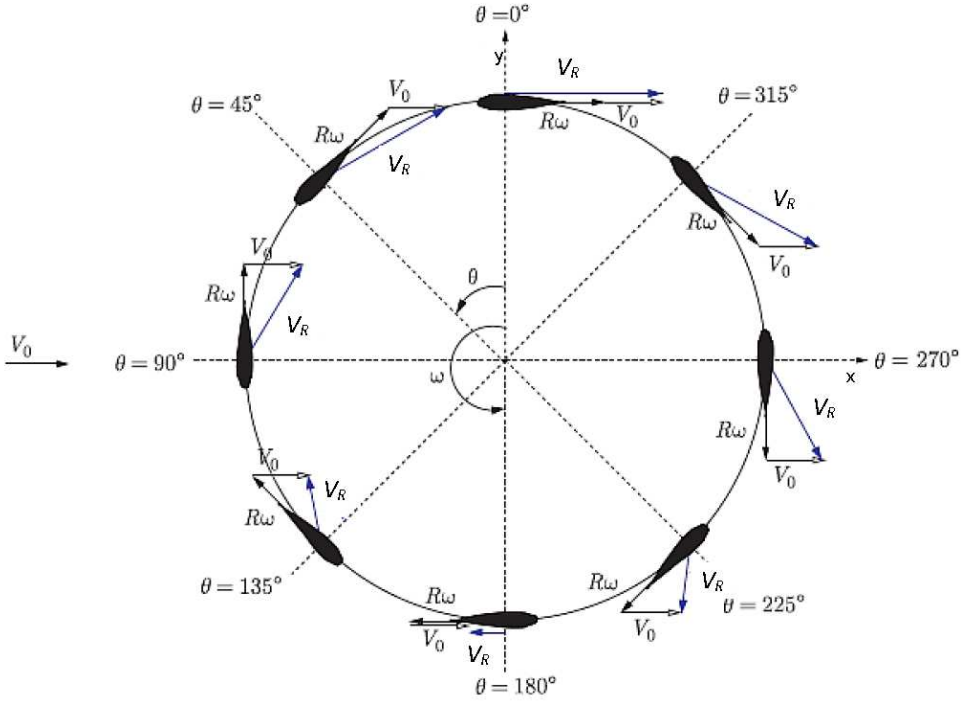

Figure 1.4: Schematic of Azimuthal Position and Velocity Triangle [7]

Tip speed ratio λ is also an important parameter, which is the ratio of the tangential velocity to the free stream velocity and expressed as,

$$\lambda = \frac{\omega R}{V_0} \tag{1.4}$$

Therefore, the relative velocity can be expressed as,

$$V_R = V_0 \sqrt{1 + 2\lambda \cos\theta + \lambda^2} \tag{1.5}$$

From geometric consideration the local angle of attack seen by the blades is given by,

$$\alpha = \arctan\left(\frac{\sin\theta}{\cos\theta + \lambda}\right) \tag{1.6}$$

Another important parameter is the solidity of the turbine σ which is defined as,

$$\sigma = \frac{Nc}{R} \tag{1.7}$$

where N is the number of the blades, c is the chord length of one blade and R is the turbine radius.

Total instantaneous torque and power coefficients of the turbine are given by,

$$C_T = \frac{T}{\rho H R^2 {V_0}^2} \tag{1.8}$$

and

$$C_P = \frac{T\omega}{\rho H R {V_0}^3} \tag{1.9}$$

respectively, where T stands for torque produced by the turbine and ω is the rotational speed of the turbine. According to equation 1.6, angle of attack α versus azimuthal position θ is shown in Figure 1.5 for different tip speed ratios λ.

In operation of Darrieus turbine, angle of attack seen by the turbine blades change significantly. Besides, for most of the λ values, incidence angle exceeds the static stall angle and this causes a phenomenon called dynamic stall. Dynamic stall is a situation containing a number of flow separations and reattachments occurring on an airfoil when it is in a rapid unsteady motion when especially static stall angle is exceeded. In Darrieus rotor type vertical axis water turbines, dynamic stall plays an important role on the turbine performance, noise and vibration [8].

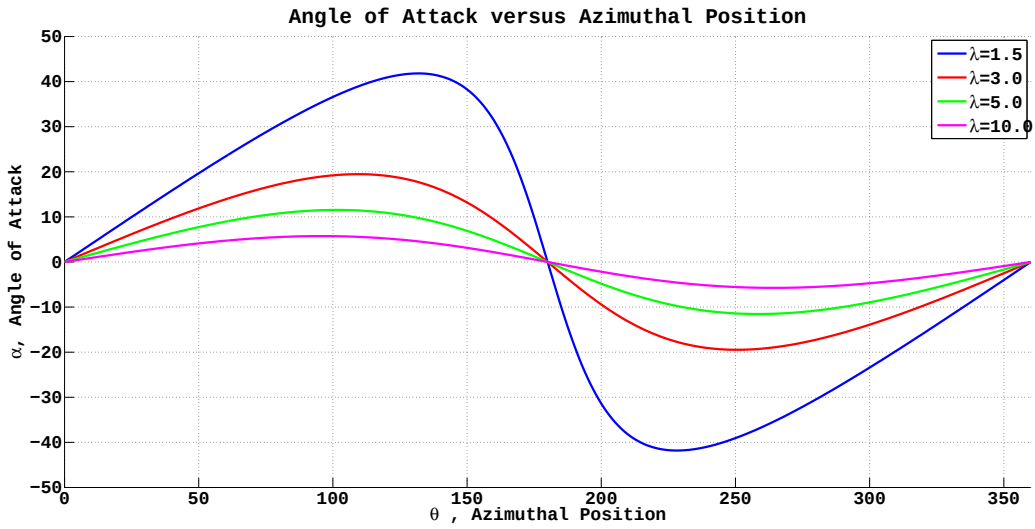

Figure 1.5: Incidence Angle α versus Azimuthal Blade Position θ

Laneville and Vittecoq [9], described reduced frequency for Darrieus turbines derived from helicopter blade theory as,

$$F^* = (\frac{c}{R})(\frac{1}{\lambda - 1})(\frac{1}{2\alpha_{max}}) \tag{1.10}$$

where α_{max} is

$$\alpha_{max} = \arctan(\frac{1}{\sqrt{\lambda^2 - 1}}) \tag{1.11}$$

For F^* values smaller than 0.05, the flow is quasisteady and for F^* values larger than 0.05, the flow is strongly affected by dynamic stall if the incidence angle seen by blades exceeds the static stall angle [10]. For Darrieus type water turbine, dynamic stall is a dominant factor due to their low tip speed ratio and high solidity ratio.

1.2 Mathematical Modeling of Darrieus Turbine

Several mathematical models are developed in the past in order to predict the performance of Darrieus turbines. As Islam et al. [11] stated, in literature most studied and best validated mathematical methods can be categorized into three groups as,

- Momentum models
- Vortex models

- Cascade model

In all these computational models, basic components are,

- Calculation of relative velocities and incidence angles in different azimuthal position of the turbine at different tip speed ratios.
- Calculation of the induced velocity taking into account the blade interactions.
- Mathematical expressions in order to calculate normal and tangential forces occurring on the turbine blades [11].

Besides these mathematical models, with the developments in computing technology Unsteady Reynolds Averaged Navier-Stokes (URANS) modeling have become very popular nowadays.

1.2.1 Momentum Models

In momentum models, basically the turbine is divided into streamtubes. The momentum model is based on the calculation of the induced velocity by equating the force on the blades with the rate of change of momentum of the fluid in each streamtube.

In 1974, Templin [12] developed single stream tube model which the most simple momentum model for the performance calculation of Darrieus turbines. In this model, the entire swept area of the turbine is enclosed by a single streamtube as shown in Figure 1.6. In 1974, Wilson and Lissaman [13] proposed multiple streamtube model which is improved interpretation of single streamtube model. In multiple stream tube model, the turbine swept area is divided into a series adjacent parallel streamtubes and in each stream tube blade element and momentum theories are applied separately as shown in Figure 1.7. In 1988, Paraschivoiu [14] developed double-multiple streamtube model in which calculations are done separately for upstream and downstream half of the turbine as shown in Figure 1.8. The double-multiple streamtube model is better than single and multiple streamtube models in correlating experimental and calculated results [11].

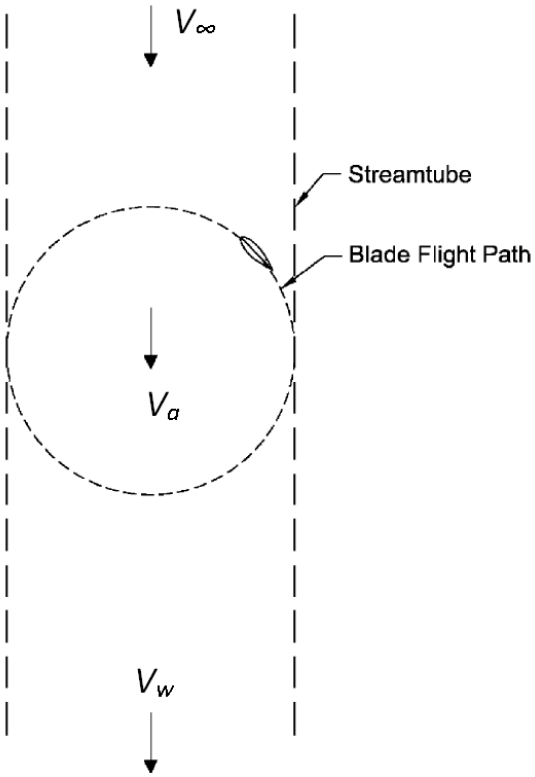

Figure 1.6: Single Streamtube Model [11]

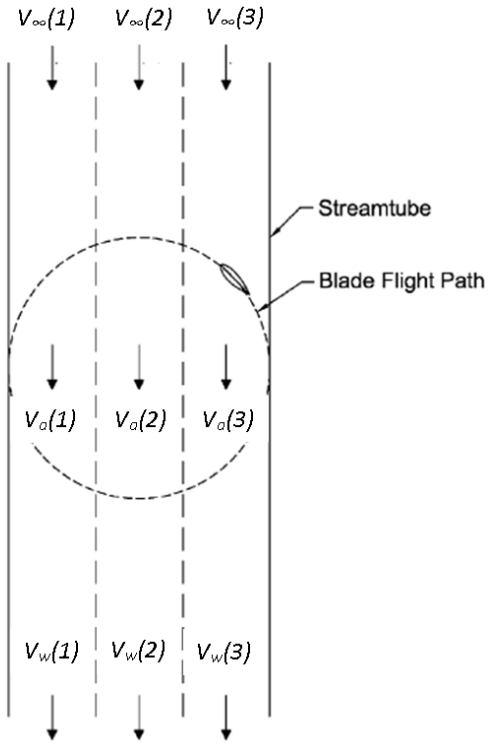

Figure 1.7: Multiple Streamtube Model [11]

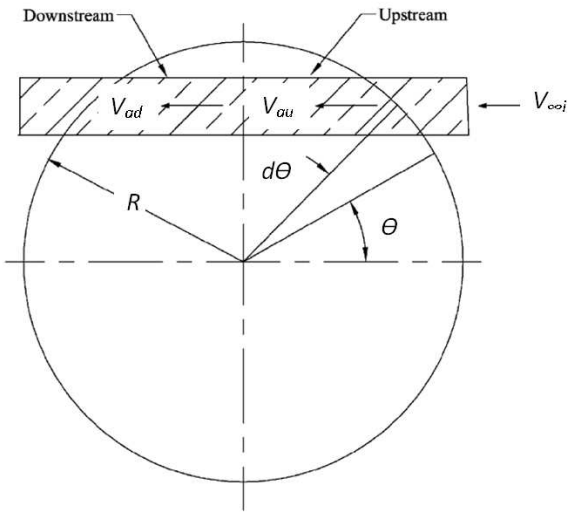

Figure 1.8: Double-Multiple Streamtube Model [11]

1.2.2 Vortex Models

The vortex models uses potential flow theory and the calculation of the velocity field about the turbine is done by the vorticity influence in the wake region of the blades of the turbine. The blades of the turbine is represented as lifting-line vortices as shown in Figure 1.9 and the strength of the vortices are determined using airfoil coefficient data sets and using calculated relative flow velocity and angle of attack. Vortex models are considered to be most accurate for most of the researchers however, its computational cost is very high [11].

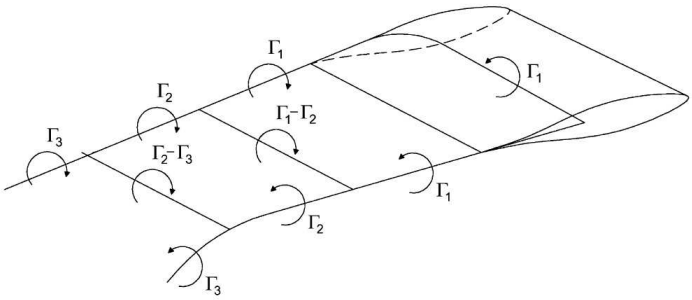

Figure 1.9: Vortex System for a Single Blade Element [11]

1.2.3 Cascade Model

Hirsch and Mandal [15] developed a cascade model for performance prediction of Darrieus turbines. Cascade principles which are widely used in turbomachineries are applied in this model. The blades of the turbine are assumed to lie in a plane surface, known as cascade, where the distance between blades is equal to the circumferential length of the turbine divided by the blade number, as shown in Figure 1.10. The cascade model gives quite well solutions for both high solidity and low solidity turbines and its computation time is reasonable [11].

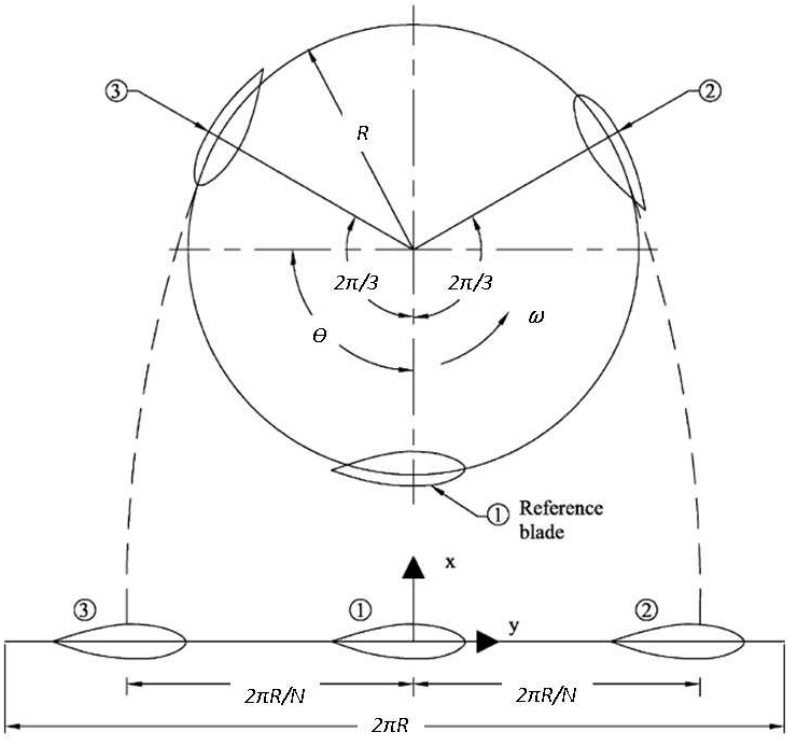

Figure 1.10: Development of Blade into a Cascade Configuration [11]

1.3 Literature Review

In literature, most of the Darrieus turbine studies focus on Darrieus wind turbines. Darrieus water/tidal turbine studies are less compared to wind turbine studies. One of the studies for Darrieus water or wind turbine contains numerical studies for performance analysis using Computational Fluid Dynamics (CFD) and other mathematical

models mentioned in section 1.2. Experimental studies for performance analysis and parametric characterization of Darrieus turbines can be considered as the other type of study for Darrieus Turbines. The other studies that should be mentioned are ones investigating dynamic stall phenomenon and wake structures and the effect of these on the performance of Darrieus turbine.

Dai and Lam [2] studied numerically a straight bladed Darrieus turbine for rotor-performance prediction using commercial URANS solver of Ansys CFX. The study initially used theoretical calculation of the performance of the turbine using double-multiple streamtube model and experimental investigation by using a scaled-down model. In numerical modeling, shear stress transport (SST) $k-\omega$ model is used for turbulence modeling. The numerical results showed good agreement with the experimental results and theoretical double-multiple streamtube calculations. Lain and Osorio [16] predicted the performance of the same marine current turbine numerically using commercial URANS solver of Ansys FLUENT and compared the results obtained with the study of Dai and Lam. In this study, SST $k-\omega$ model is used for turbulence modeling, too. The study concludes that the developed model can effectively predict hydrodynamic performance. Li and Calisal [17] studied three-dimensional and arm effects on modeling vertical axis Darrieus tidal turbine. A vortex method code DVM-UBC is used for two-dimensional and three-dimensional models to study three-dimensional effects. Both two-dimensional and three-dimensional numerical results are compared with the experimental results. The results shows that the three-dimensional effects are significant when the turbine height is less than two times the radius of the turbine and negligible when the turbine height is more than seven times the radius of the turbine. Alidadi [6] improved DVM- UBC code that is used in study of Li and Calisal [17] in order to predict the performance of ducted vertical axis turbines and this new numerical code is named as BEM-DVM. An optimization study is done in order to find the optimum duct shape for getting maximum power output from the turbine. The results showed that using ducts for turbine improves the power coefficient and it also decreases torque fluctuations significantly. A 2D numerical study is carried out by Nabavi [18] and numerical results are compared with experimental results. It is mentioned that numerical results show good agreement with the experimental ones using Spalart Allmaras turbulence model. Malipeddi and Chatterjee [19]

examined also the influence of duct geometry on Darrieus turbine performance. In this study, 2D numerical study on ducted Darrieus turbine is performed using SST $k-\omega$ turbulence model. It is stated that using a duct for the operation of the turbine, reduces the torque ripple and increases the turbine performance significantly. Gretton et al. [20] studied a small scale prototype of a 15 kW tidal turbine numerically using Ansys CFX solver. 2D parametric study is performed numerically using SST $k-\omega$ turbulence model and the results are compared with the baseline turbine. Another 2D numerical study is carried out by Almohammadi et al. [21] considering the mesh independency techniques for vertical axis Darrieus wind turbines. The study investigates the mesh refinement methods, namely General Richardson Extrapolation (GRE), Grid Convergence Index (GCI), and the fitting method while using transition SST and RNG $k-\epsilon$ turbulence models in modeling. It is stated that mesh independent solutions obtained by GRE method is promising. Another important work done by Almohammadi et al. [22] is the sensitivity analysis of vertical axis wind turbine CFD. In this research, effect of meshing on predicted power coefficient of the turbine is analyzed by investigating the effects of cell type, aspect ratio of the cell on the blade surface and the total number of cells in the domain. In addition, the effect of time step and turbulence intensity are examined for the simulation phase. It is stated that using quadrilateral cells in computational domain for VAWT analysis is better, since usage of triangular cells may cause numerical diffusion. In addition, decreasing the cell aspect ratio on the blade surface is an important factor in 2D numerical solution of VAWTs.

Rawlings [1] studied parametric characterization of a vertical axis Darrieus type tidal turbine experimentally. Experiments are conducted in University of British Colombia (UBC) towing tank and a parametric study was conducted which examines the effects of parasitic drag, cambered blades, angle of attack, tip losses and shaft fairing on turbine performance. The effects of each characteristic on overall efficiency of the turbine are quantified, leading to predict for the maximum efficiency of the turbine without losses. Kyozuka [23] studied a Darrieus-Savonius turbine experimentally. Since Darrieus turbine has small starting torque a hybrid turbine, composed of Darrieus and Savonius turbine rotors, is proposed. Semi-circular buckets with four different configurations are used for the Savonius rotor part and torque study is performed

in circulating water channel. Combined turbine was tested in circulating water channel and the effect of attaching angle between Savonius rotor and Darrieus wings was studied. In addition, power generation studies of the combined turbine are performed in a towing tank and power coefficients were compared with the experiments conducted in circulating water channel. The study showed that combined turbine has improvement in the starting torque. On the other hand, at high rotational velocity ratio (tip speed ratio) maximum torque is decreased by 30 % compared to the torque generated by the solo Darrieus turbine. Shiono et al. [24] also studied a Darrieus water turbine experimentally. In this study, experiments are conducted in circulating water channel and optimum solidity ratio and number of blades are examined. The optimum solidity for three bladed turbine is stated. Furthermore, It is concluded that, the efficiency for a three bladed turbine is less than a two bladed one for a constant solidity. However, the ability for self starting is improved with increasing number of blades.

Dynamic stall is a complex phenomenon that effects the performance, noise and vibration of vertical axis turbines seriously. One of the tools that is used to investigate dynamic stall is CFD. Nobile et al. [25], studied dynamic stall for 2-D flow around Vertical Axis Wind Turbine blades using different turbulence models. The numerical results are compared with the available data on the subject. This study shows that the $k - w$ SST (Shear Stress Transport Turbulence Model) can predict the dynamic stall better than the other turbulence models.

Wang et al. [8] also studied the dynamic stall phenomenon in unsteady 2D flow over the NACA0012 airfoil at a Reynolds number of order 10^5 numerically. In this study, standard $k - w$ and SST $k - w$ turbulence models are employed. The results obtained from numerical study are compared with the corresponding experimental data. It is concluded that the characteristics of dynamic stall is well captured by the SST $k - w$ turbulence model and the SST $k - w$ model can predict the experimental results with reasonable accuracy better than standard $k - w$ model. However, the two models suffer from capturing the flow characteristics at very high angles of attack where fully detached flow occurs and 3D effects are more significant. Allet et al. [26] studied 2D numerical solution of a single bladed VAWT with NACA 0015 blade. Two

turbulence models, Cebeci-Smith and Johnson-King, are employed with a finite element turbulent solver. The normal and tangential forces are similar to experimental results but the maximum values are over-predicted. In another work of Wang et al. [27] previous study is extended and transition SST, RNG $k-\epsilon$ turbulence models and Detached Eddy Simulation (DES) is employed in order to investigate the dynamic stall. Numerical results are compared with the experimental results and DES coupled with SST k-ω model showed good agreement with the experiments. Ferreira et al. [28] studied 2D numerical simulation of a single bladed (NACA 0015) VAWT using Spalart-Allmaras and $k-\epsilon$ turbulence models and Large Eddy Simulation (LES) and Detached Eddy Simulation (DES) models. The results are compared with the previously performed experiments [29] . It is expressed that DES is the most accurate one capturing the dynamic stall characteristics. It is also pointed that LES performs worse than DES model, due to less accurate modeling of the wall region.

1.4 Outline of the Thesis Study

In Chapter 2, two-dimensional CFD modeling of an experimental Darrieus turbine is presented. The results obtained from different turbulence models are compared with the available experimental data. In Chapter 3, design of a Darrieus water turbine for river applications is presented and the average power coefficient results obtained from double-multiple streamtube code QBlade are compared with two dimensional CFD model results. In the last chapter, Chapter 4, the results and findings of the study are summarized.

CHAPTER 2

CFD MODELING OF DARRIEUS TURBINES

2.1 Validation and Verification of 2D Numerical Solution

For validation and verification purposes, the turbine presented by Maitre et al. [10] has been used for CFD modeling and the power coefficients obtained are compared with the experimental power coefficients. Two-dimensional (2D) numerical simulation of the turbine is performed by Ansys Fluent URANS solver.

2.1.1 Experimental Set-Up

The experiments are done in hydrodynamic tunnel available in The Laboratory of Geophysical and Industrial Flows (LEGI). The test section dimensions are 1000 mm in length, 700 mm in width and 250 mm in height. View of the experimental set up is shown in Figure 2.1. The turbine is made of three straight NACA 0018 blades with a chord length of 32 mm and they are equally spaced in the azimuthal plane. The turbine height is 175 mm and it contains a 22 mm shaft in diameter holding the blades from their centers. The diameter of the turbine is 175 mm and the blades are modified such that the camber line conforms with the circular path of the blades. The geometric specifications of the turbine are given in Table 2.1. The free stream velocity is 2.8 m/s with a turbulence intensity of 2 % [10].

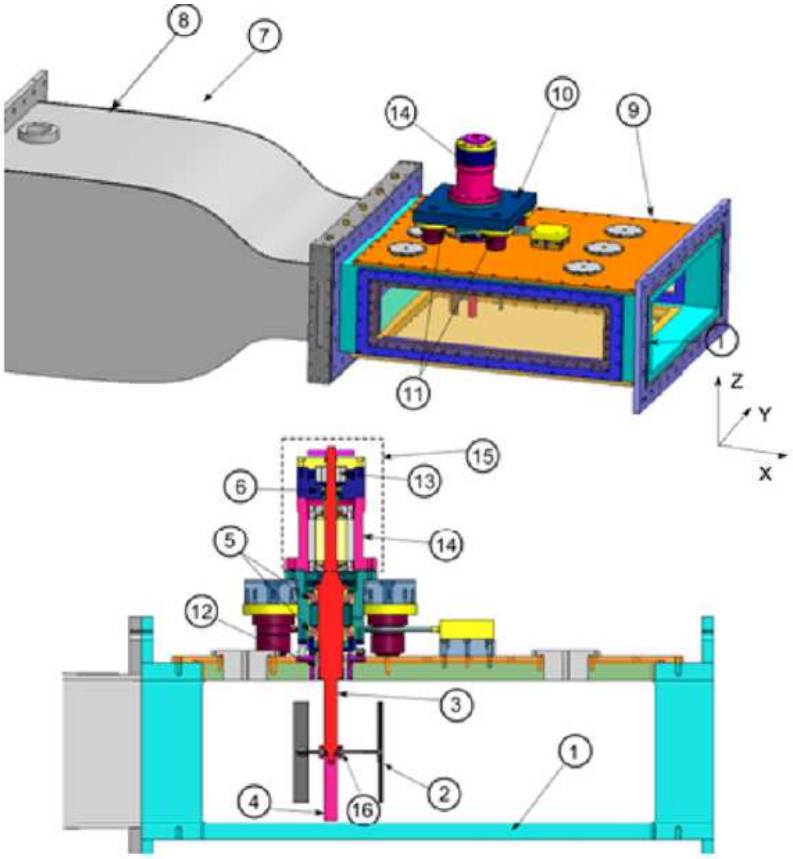

Figure 2.1: View of The Experimental Setup [10]

Table 2.1: Geometric Specifications of the Turbine

Blade's profile	NACA 0018
Chord Length	32 mm
Number of Blades	3
Turbine Height	175 mm
Turbine Diameter	175 mm
Shaft Diameter	22 mm

2.1.2 Problem Domain and Grid Generation

Schematic view of the 2D calculation domain is shown in Figure 2.2. The sizes of the domain are selected according to the domain size independency study performed by McLaren [30] and Nabavi [18]. The left hand side boundary of the rectangle is set as the velocity inlet, whereas, the right hand side is set as the pressure outlet where the pressure is atmospheric pressure. The upper and lower boundaries are set to be no-slip walls in order to represent the water tunnel walls. The circular ring part of the

domain is the rotating domain while the outer and inner domains are stationary. The interface between the stationary and rotating domain is modeled by the sliding mesh model (SMM).

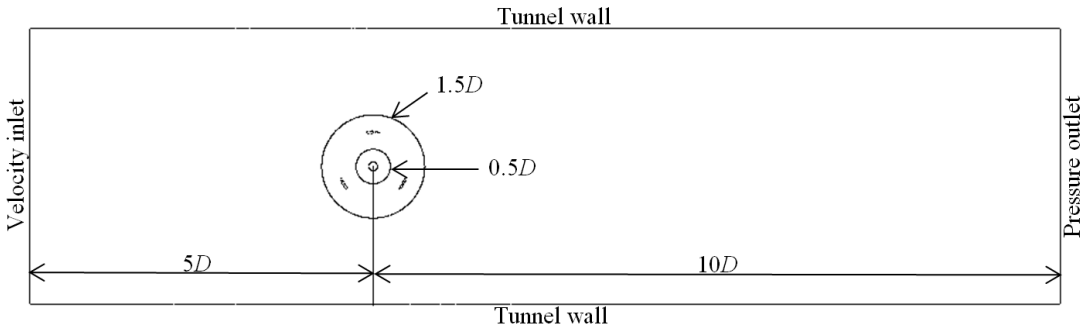

Figure 2.2: Schematic View of the Calculation Domain

Since flow dynamics of Darrieus turbine is complex due to flow separations and reattachments occurring on the blades, meshing of the domain is one of the key points. When such flow characteristics are present, using structured mesh rather than unstructured mesh shows better performance for the accuracy and stability of the solution [31]. However, the usage of structured mesh in the analysis of VAWTs is difficult. Thus, structured mesh is used only on airfoil surfaces and outer stationary domain. In the rotating domain, quadrilateral cells are used, since they are known to be more stable due to low numerical diffusion [21]. In the airfoil boundary layer, structured mesh is created ensuring y^+ value near 1 with a fixed growth rate of 1.05. This y^+ value near 1 is required in order to ensure that the first node is located in the viscous sublayer for turbulence models not using wall functions such as $k-\omega$ SST and transition SST models [32]. y^+ is a non-dimensional value describes the relative distance of the first node from wall surface and it is expressed as,

$$y^+ = \frac{\rho u_* y}{\mu} \tag{2.1}$$

where y is distance to nearest wall (node distance to wall) and u_* is the friction velocity at the nearest wall defined by

$$u_* = \sqrt{\frac{\tau_w}{\rho}} \tag{2.2}$$

where τ_w is wall shear stress and given as,

$$\tau_w = C_f \frac{1}{2} \rho V_0^2 \tag{2.3}$$

where C_f is skin friction coefficient. The skin friction coefficient is estimated by the Schlichting skin friction coefficient formula expressed as [33],

$$C_f = [2\log_{10}(Re_x) - 0.65]^{2.3} \tag{2.4}$$

which is valid for $Re_x < 10^9$. The first cell height, y, is evaluated based on chord Reynolds number which is given by,

$$Re_c = \frac{\rho c \omega R}{\mu} = \lambda \frac{\rho c U_0}{\mu} \tag{2.5}$$

where μ is dynamic viscosity of water and c is the chord length.

The structured boundary layer mesh around airfoil is shown in Figure 2.3 and mesh of the rotating domain is shown in Figure 2.4.

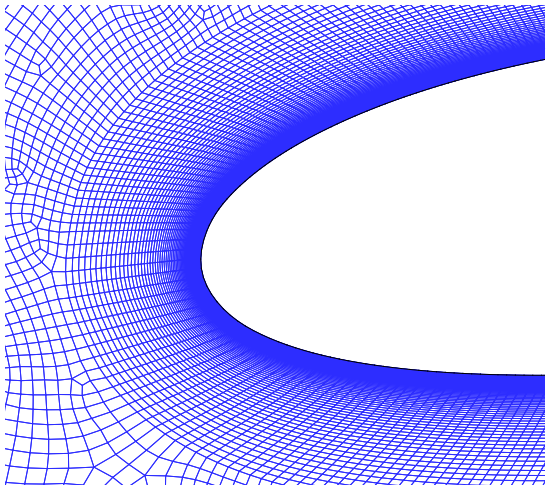

Figure 2.3: Structured Mesh Around Blade

2.1.3 Numerical Simulation

2D numerical simulation is performed by ANSYS Fluent a commercial software capable of solving Unsteady Navier Stokes equations. The SIMPLE algorithm is used for pressure velocity coupling. The simulations are started with first order upwind discretization scheme for both space and time, after the first rotation of the turbine temporal and spatial discretization scheme is set to second order upwind scheme. After sixth or seventh rotation torque produced by turbine becomes periodic and the

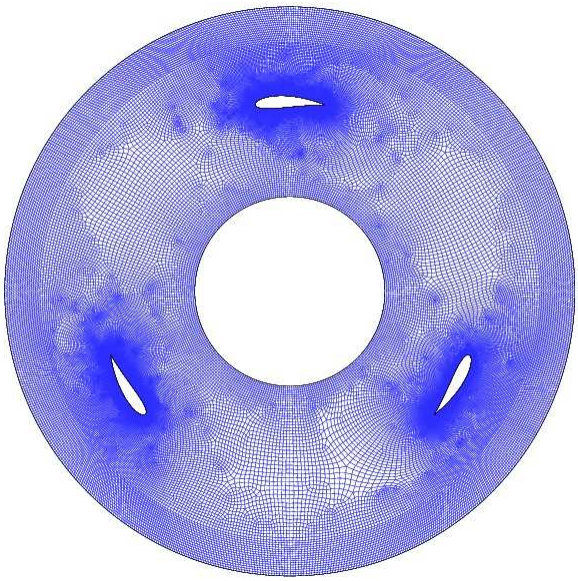

Figure 2.4: Rotating Domain Mesh

results presented are taken from the tenth rotation. k-ω SST turbulence model is employed for turbulence modeling since it shows better performance for complex flows including adverse pressure gradients and flow separations like in VAWTs as mentioned in Section 1.3. The numerical simulation parameters is shown in Table 2.2. For validation purposes, the tip speed ratio $\lambda = 1.5$ with corresponding rotational

Table 2.2: Numerical Modeling Parameters

Pressure Velocity Coupling Scheme	Green-Gause Node Based
Gradient	Second Order
Pressure	Second Order Upwind
Momentum	Second order Upwind
Turbulent Kinetic Energy	Second Order Upwind
Specific Dissipation Rate	Second Order Upwind
Transient Formulation	Second Order Implicit

speed $\omega = 48$ rad/s is selected for the case study. The $\lambda = 1.5$ case is selected since the angle of attack seen by blades exceeds the static stall angle and dynamic stall is dominant in this condition.

2.1.3.1 Time Step Independency

The flow over Darrieus turbine is periodic and a proper time step selection is important in order to ensure the solution is independent of the time step. The time step corresponds to one degree rotation of the turbine is expressed as,

$$\Delta t = \frac{\pi}{180\omega} \tag{2.6}$$

The time steps used for time step independence study correspond to 1°, 0.5° and 0.25° rotation and they are shown in Table 2.3. The total number of cells for the grid of the problem domain is 266000.

Table 2.3: Time Steps Used for Time Step Independency

Time Step (s)	Corresponding Degree of Rotation (degree)
0.00036361026	1
0.00018180513	0.5
0.00009090256	0.25

The results are shown in Figure 2.5. As can be seen from Figure 2.5, the three time steps almost give the same results. For 0.25° rotation time step, computational cost is high. On the other hand, for 1° rotation time step, the number of iterations in each time step is high. Thus, 0.5° rotation time step is selected for further analysis.

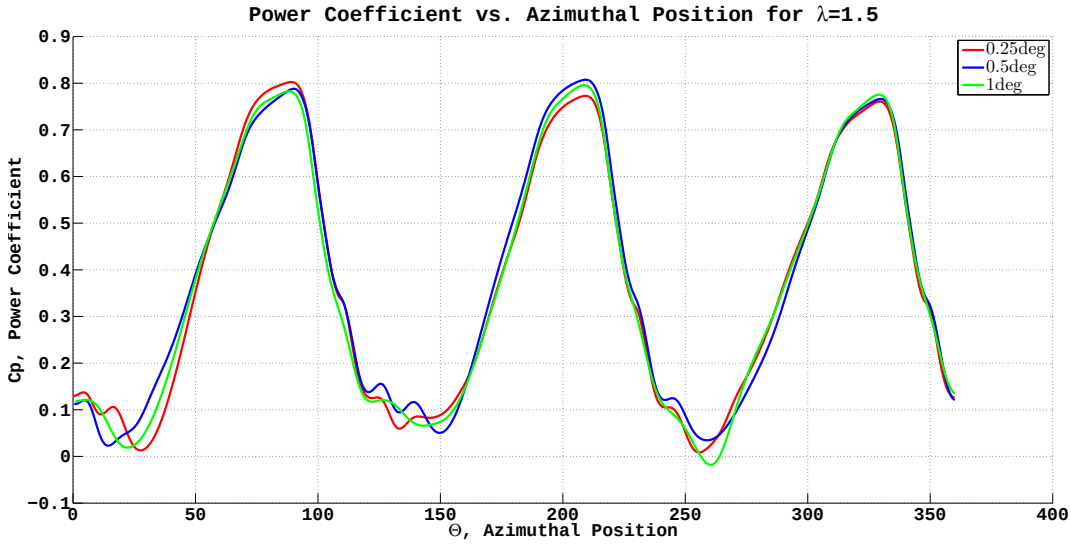

Figure 2.5: The Variation of Power Coefficient with Different Time Steps

2.1.3.2 Residual Independency

The mesh used in residual independency study is the same as the one used in Section 2.1.3.1. For residual independency study, the residuals are set to be $5x10^{-5}$, $1x10^{-5}$ and $5x10^{-6}$ for all variables and the time step is set to 0.5° rotation time step. The results are shown in Figure 2.6. After evaluating the results of Figure 2.6, the resid-

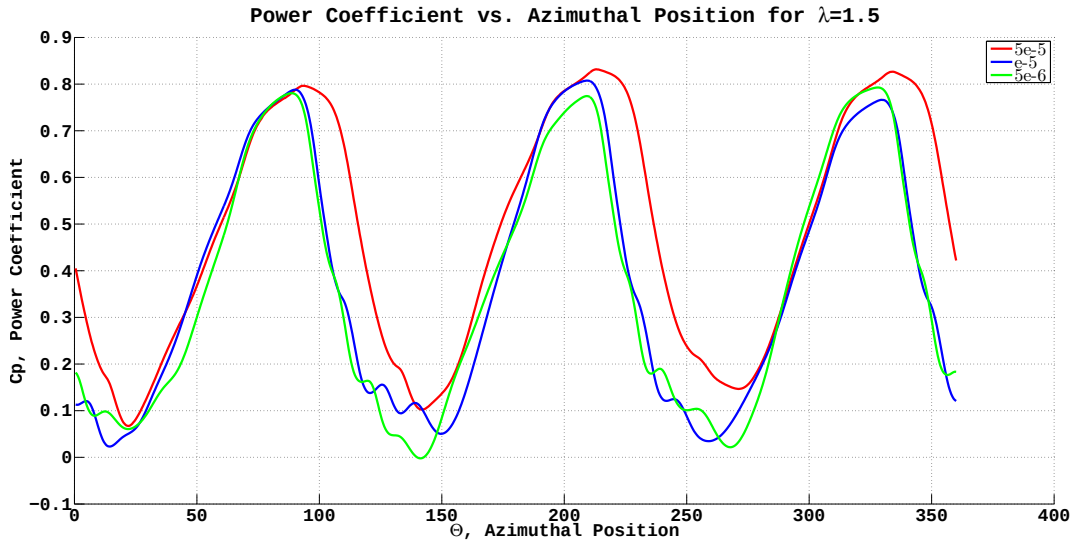

Figure 2.6: The Variation of Power Coefficient with Different Residuals

uals are decided to set to $1x10^{-5}$, since using $5x10^{-5}$ does not produce satisfactory results and computational cost is high when $5x10^{-6}$ is used for the residuals.

2.1.3.3 Mesh Independency

Three meshes are generated for mesh independency study namely coarse, medium and fine. The number of elements in these meshes are shown in Table 2.4.

Table 2.4: Number of Elements for Mesh Independency Study

Mesh Type	Number of Elements
Coarse	156213
Medium	218158
Fine	333703

The time step and the residuals are set as decided in Sections 2.1.3.1 and 2.1.3.2. The

grid of the rotating domains for coarse, medium and fine meshes are shown in Figure 2.7 and near blade meshes are shown in Figure 2.8.

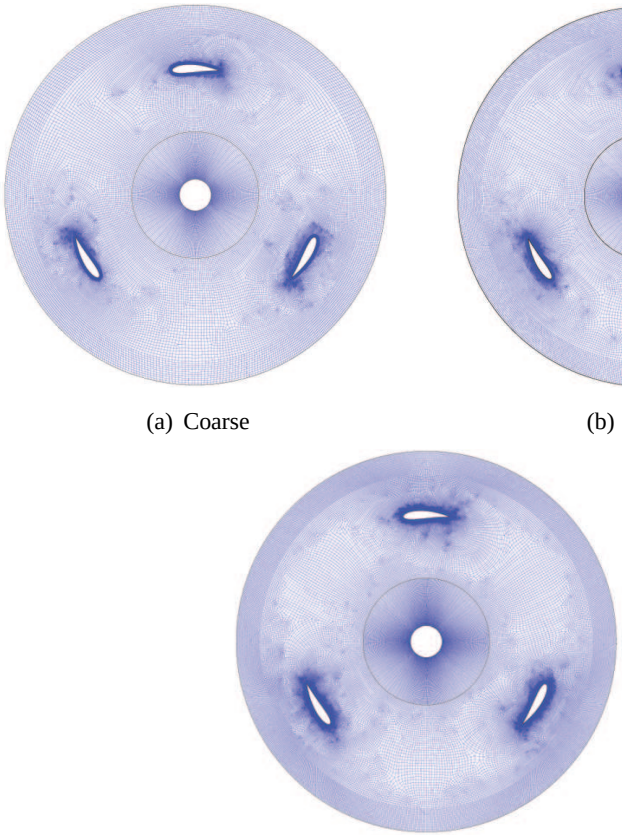

(a) Coarse (b) Medium

(c) Fine

Figure 2.7: Rotating Domain Meshes

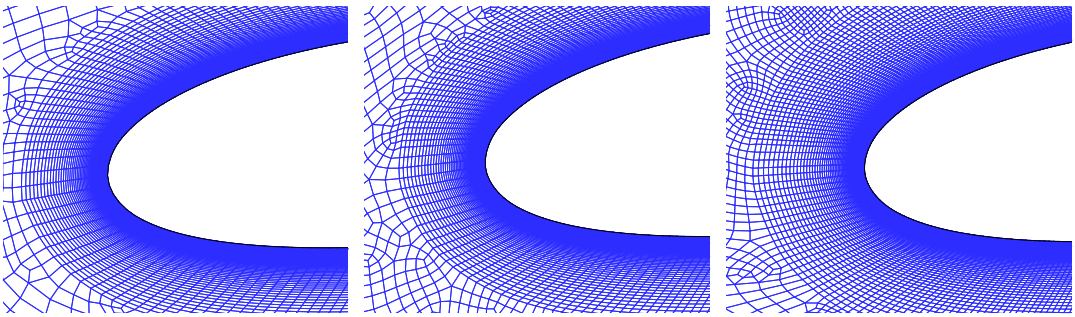

(a) Coarse (b) Medium (c) Fine

Figure 2.8: Near Blade Meshes

The coefficient of performance versus azimuthal position of different meshes are shown in Figure 2.9. Although, the medium and fine mesh show similar pattern as

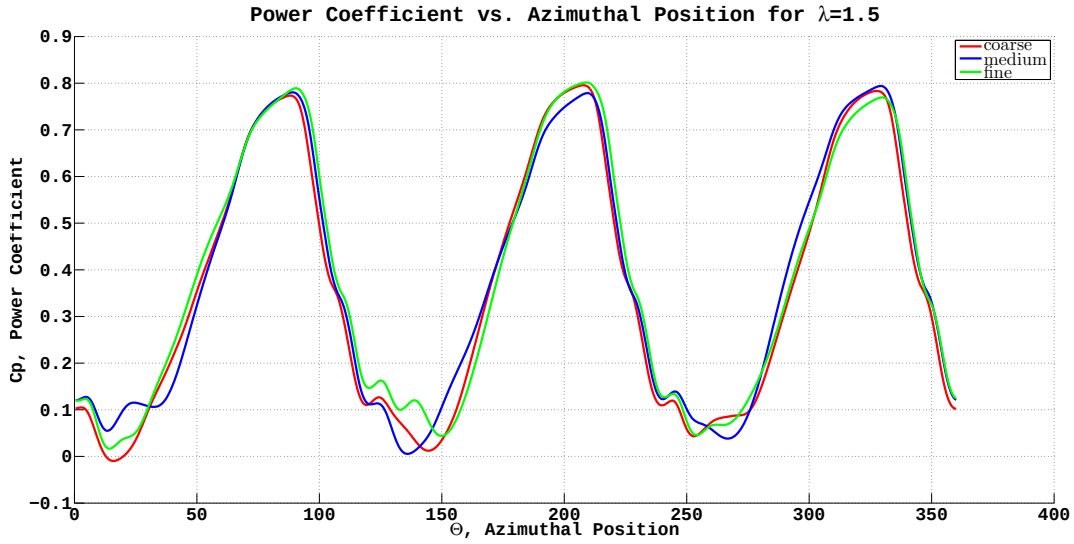

Figure 2.9: The Variation of Power Coefficient with Different Meshes

can be seen from Figure 2.9, they differ from each other in especially azimuthal positions between 100° and 150°. For this reason, a moderate mesh is created having a number of elements around 266000 which is the same as the mesh used in time step and residual independency studies. The comparison between moderate and fine mesh is shown in Figure 2.10. The moderate mesh created fits better to fine mesh results than medium mesh. Thus, moderate mesh is used for further analysis.

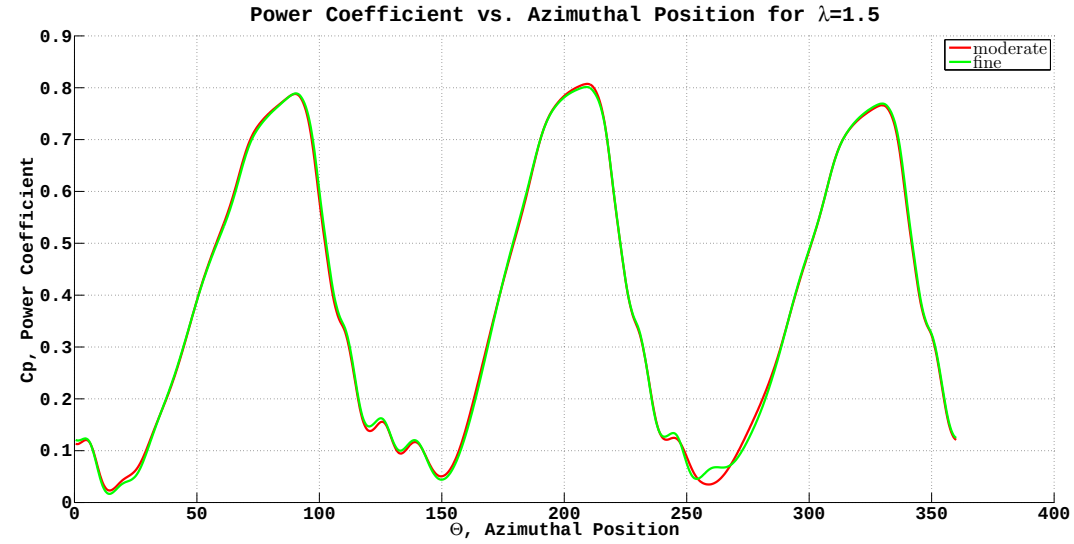

Figure 2.10: Comparison between Moderate and Fine Meshes

2.1.3.4 Flow Field Analysis

The power coefficient change with azimuthal position for the first blade for $\lambda = 1.5$ is shown in Figure 2.11. In the figure, the variation of the power coefficient with azimuthal position for $k-\omega$ SST, realizable $k-\epsilon$ with enhanced wall treatment and Spallart Almaras turbulence models are presented and the results are also compared with the numerical results obtained by Maitre et al. [10].

It is observed that the power coefficient increases approximately until 90° azimuthal position and then decreases until 150° azimuthal position is reached for all three turbulence models. The power coefficient also remains at a constant value of zero between 150° and 270°. After 270° azimuthal position, there is some increase and then decrease in the power coefficient until 360°. In addition, the main power production occurs between 0° and 150° azimuthal positions for the first blade. Then the second blade repeats the motion of the first blade and the power production is completed with the same motion of the third blade for one rotation of the turbine.

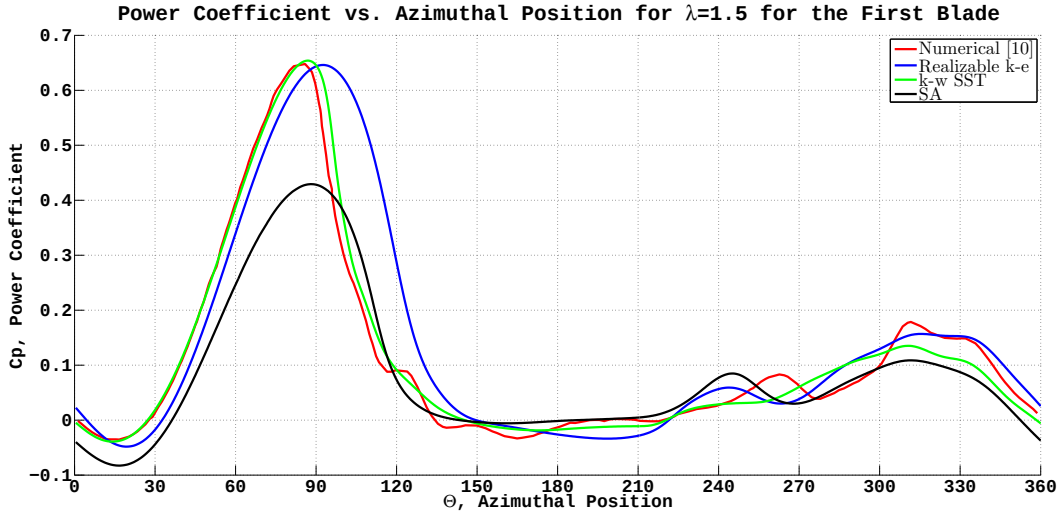

Figure 2.11: Power Coefficient Variation for the First Blade at $\lambda = 1.5$

The vorticity fields of the first blade between angles 0° and 120° azimuthal positions with 15° increment are shown in between Figures 2.12 and 2.20 for all three turbulence models. Since the vorticity field around the blades are the same for 0° and 120° azimuthal positions, the vorticity fields are given only between 0° and 120°.

Figure 2.11 shows that, between 0° and 90° azimuthal positions, the power coefficients obtained from $k-\omega$ SST turbulence model have highest value while Spalart Allmaras turbulence model results are the smallest and $k-\epsilon$ turbulence model results lie in between those. When the vorticity fields between 0° and 90° azimuthal positions are analyzed, as shown in Figures 2.12 through 2.18, it is observed that the positive vorticity in the pressure side of the first blade is widest for Spalart Allmaras turbulence model and $k-\epsilon$ turbulence model has wider vorticity than $k-\omega$ SST turbulence model. For this reason, it can be said that the power coefficient obtained might be relevant with the width of vorticity in the pressure side of the blade between 0° and 90° azimuthal positions and this situation may be expressed as the width of vorticity in the pressure side of the first blade increases, the power coefficient obtained becomes smaller.

It is also worth mentioning that the vortex shedding around the shaft is well modeled by $k-\omega$ SST and Spalart Allmaras turbulence models; however, the vortex shedding is not captured well by $k-\epsilon$ turbulence model as can be seen in Figures 2.12 through 2.20.

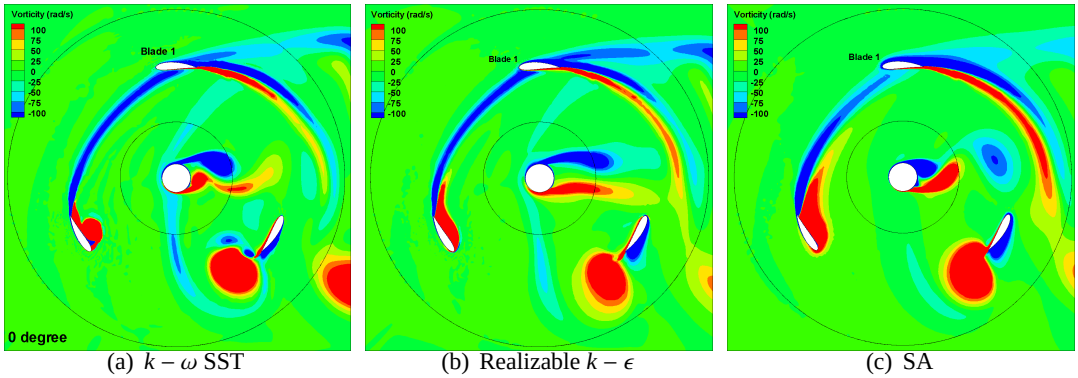

(a) $k-\omega$ SST (b) Realizable $k-\epsilon$ (c) SA

Figure 2.12: Vorticity Contours at 0° for $\lambda = 1.5$

The streamlines between 60° and 120° azimuthal positions with 15° increment are shown in Figures 2.21 through 2.25 and the streamlines of three turbulence models are compared.

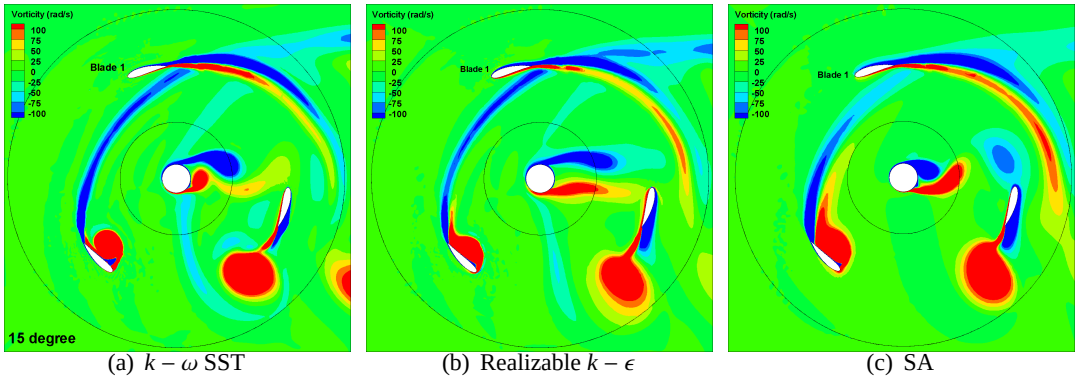

(a) $k-\omega$ SST (b) Realizable $k-\epsilon$ (c) SA

Figure 2.13: Vorticity Contours at 15° for $\lambda = 1.5$

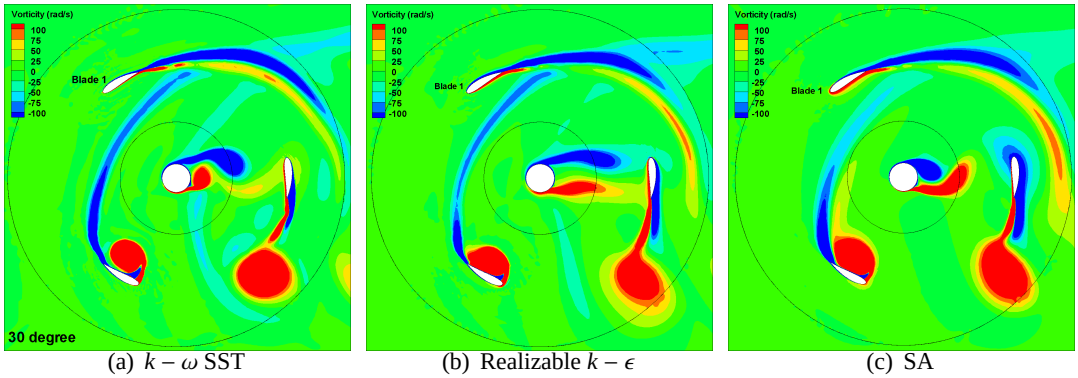

(a) $k-\omega$ SST (b) Realizable $k-\epsilon$ (c) SA

Figure 2.14: Vorticity Contours at 30° for $\lambda = 1.5$

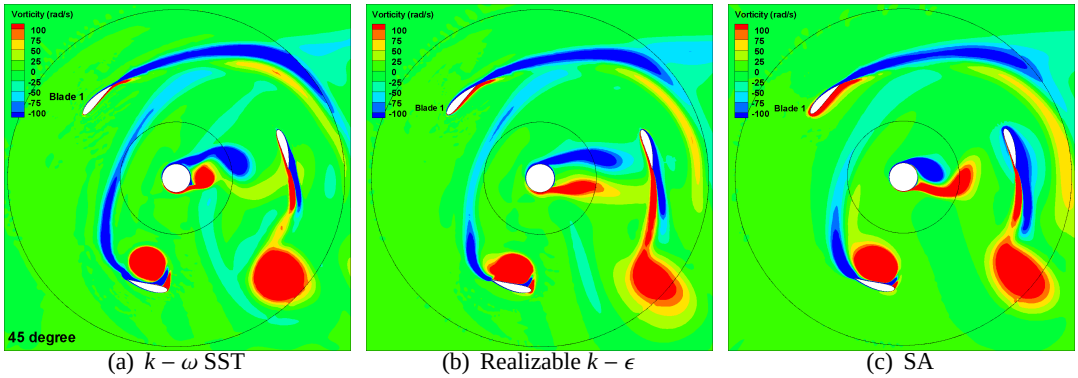

(a) $k-\omega$ SST (b) Realizable $k-\epsilon$ (c) SA

Figure 2.15: Vorticity Contours at 45° for $\lambda = 1.5$

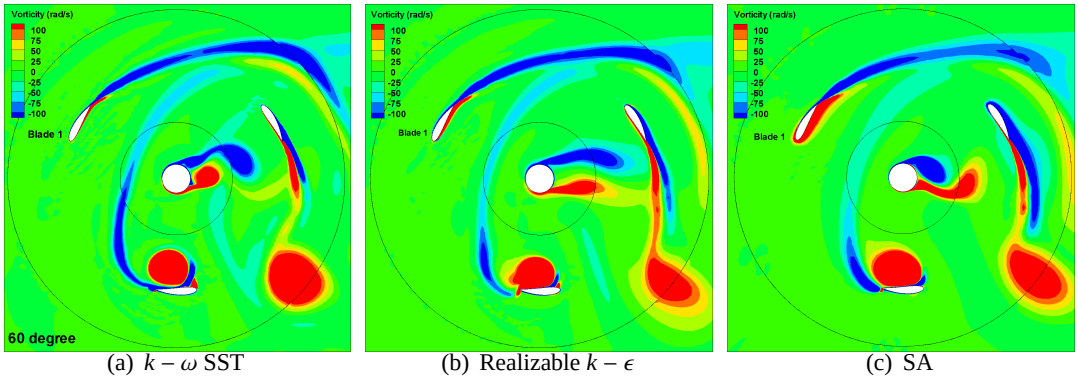

(a) $k-\omega$ SST (b) Realizable $k-\epsilon$ (c) SA

Figure 2.16: Vorticity Contours at 60° for $\lambda = 1.5$

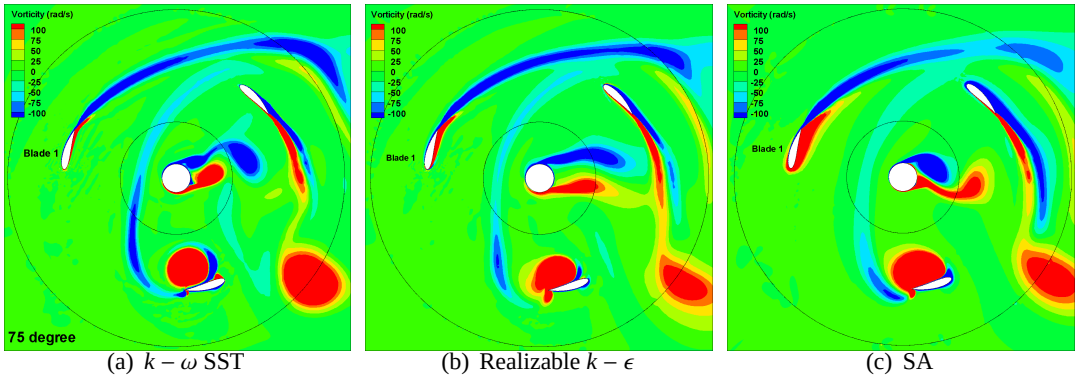

(a) $k-\omega$ SST (b) Realizable $k-\epsilon$ (c) SA

Figure 2.17: Vorticity Contours at 75° for $\lambda = 1.5$

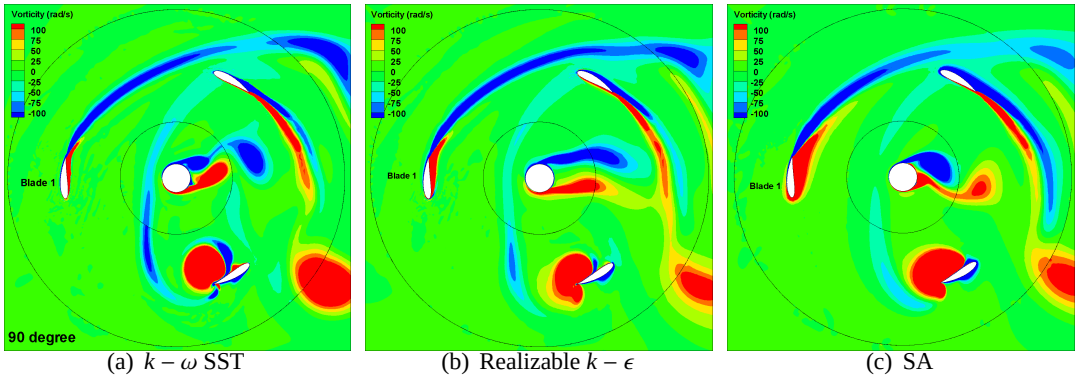

(a) $k-\omega$ SST (b) Realizable $k-\epsilon$ (c) SA

Figure 2.18: Vorticity Contours at 90° for $\lambda = 1.5$

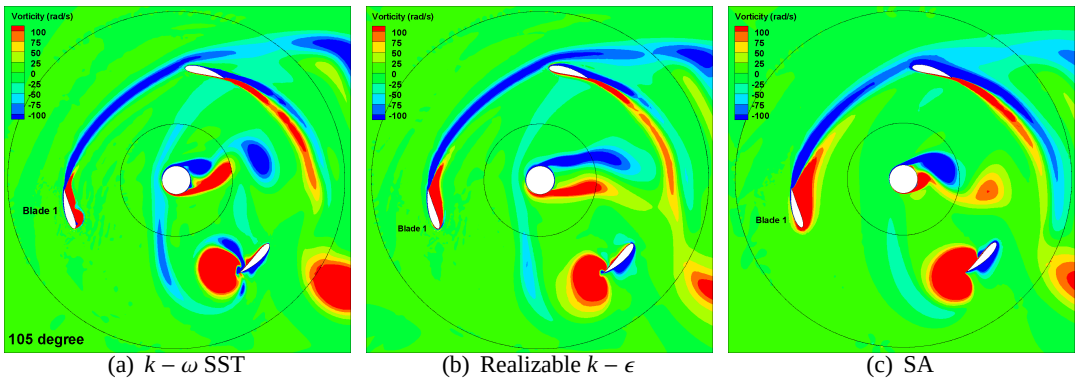

(a) $k-\omega$ SST (b) Realizable $k-\epsilon$ (c) SA

Figure 2.19: Vorticity Contours at 105° for $\lambda = 1.5$

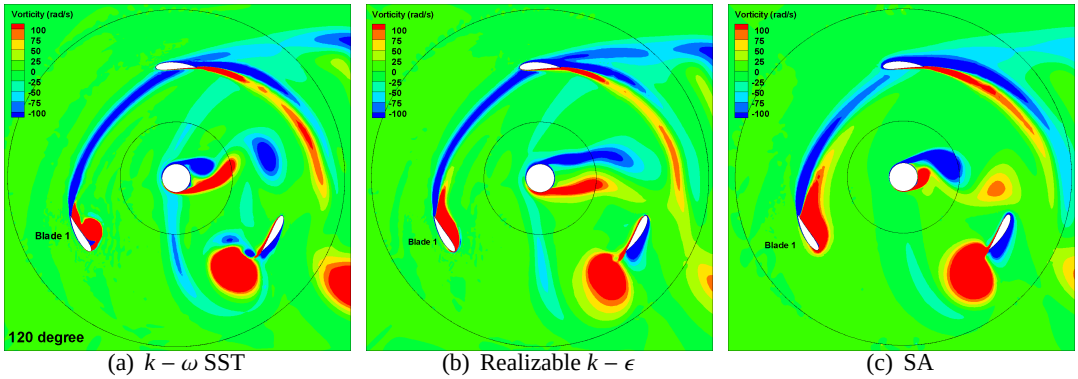

(a) $k-\omega$ SST (b) Realizable $k-\epsilon$ (c) SA

Figure 2.20: Vorticity Contours at 120° for $\lambda = 1.5$

In 60° azimuthal position, separation bubble starts to form for all the turbulence models as shown in Figure 2.21. The sizes of the separation bubbles are nearly the same for $k-\omega$ SST and Spalart Allmaras turbulence models while the size of the bubble is smaller in $k-\epsilon$ turbulence model.

When 75° azimuthal position is reached, the sizes of the bubbles increase as shown in Figure 2.22 and the size for $k-\epsilon$ model is smallest and the size for Spalart Allmaras turbulence model is larger than $k-\omega$ SST model.

In 90° azimuthal position, separation bubble obtained in Spalart Allmaras turbulence model disappears and the separation bubble for $k-\omega$ SST turbulence model is larger than $k-\epsilon$ model. From Figure 2.11, it can be seen that the power coefficient obtained by $k-\epsilon$ model shifts a little to the right in upper peak value near 90° azimuthal position. When the streamlines of these turbulence models between 60° and 90° azimuthal positions are analyzed, it can be said that $k-\epsilon$ turbulence model predicts separation later than $k-\omega$ SST and Spalart Allmaras turbulence models. Therefore, the shift of the power coefficient curve for $k-\epsilon$ turbulence model to the right might be related with its late separation estimation.

The streamlines for 105° and 120° azimuthal positions are shown in Figures 2.24 and 2.25, respectively. In 105° azimuthal position, $k-\omega$ SST has larger separation bubble than $k-\epsilon$ model while Spalart Allmaras turbulence model does not predict any. In 120° azimuthal position, Spalart Allmaras turbulence model predicts smallest bubble near the blade and the separation bubble for $k-\omega$ SST is larger than $k-\epsilon$ model. In Figure 2.11, it is also observed that the power coefficient curve of $k-\omega$ SST model faces a sharper drop compared to the other turbulence model curves after 90° azimuthal position. Hence, it is thought that this sharp drop might be related to the size of separation bubble predicted.

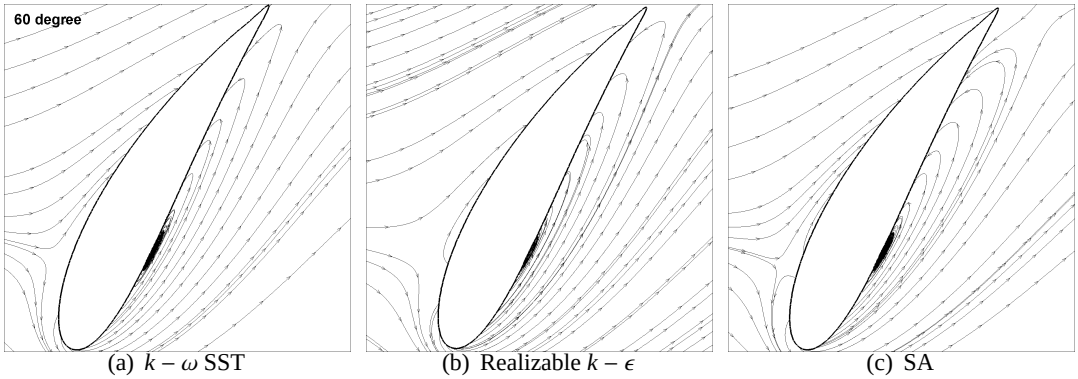

(a) $k-\omega$ SST (b) Realizable $k-\epsilon$ (c) SA

Figure 2.21: Streamlines at 60° for $\lambda = 1.5$

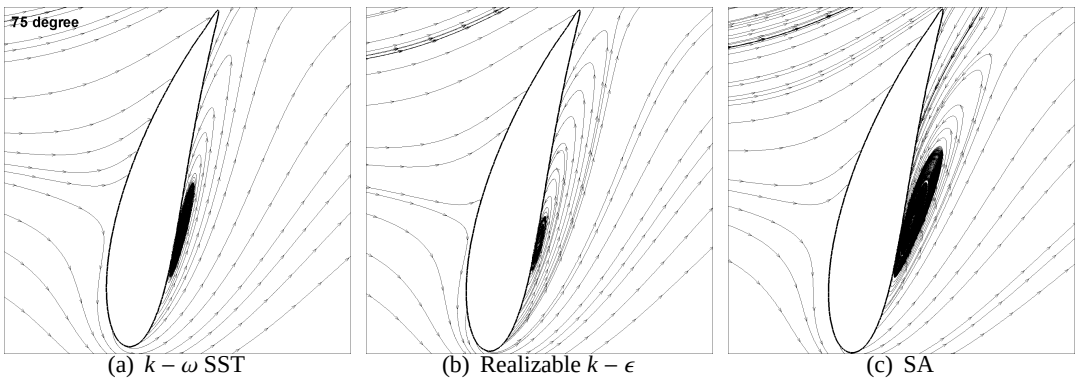

(a) $k-\omega$ SST (b) Realizable $k-\epsilon$ (c) SA

Figure 2.22: Streamlines at 75° for $\lambda = 1.5$

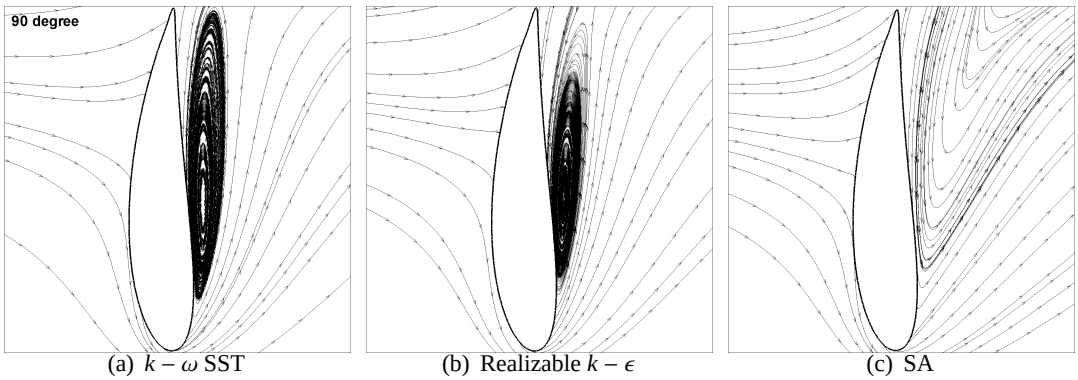

(a) $k-\omega$ SST (b) Realizable $k-\epsilon$ (c) SA

Figure 2.23: Streamlines at 90° for $\lambda = 1.5$

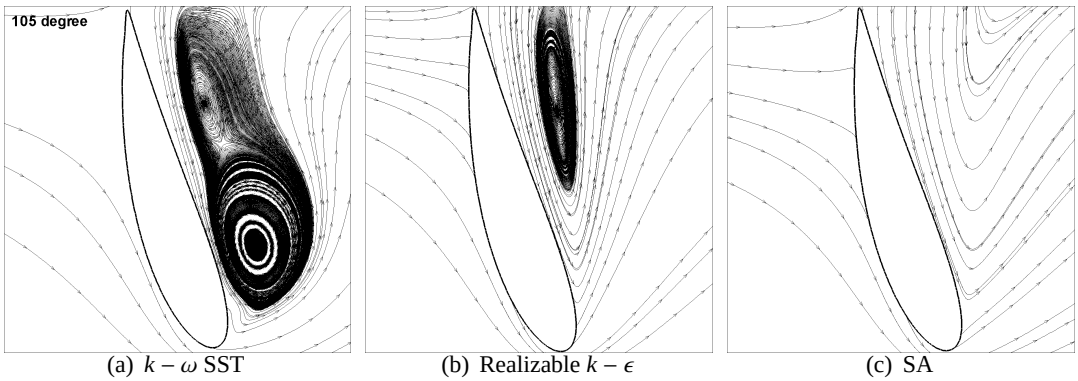

(a) $k - \omega$ SST (b) Realizable $k - \epsilon$ (c) SA

Figure 2.24: Streamlines at 105° for $\lambda = 1.5$

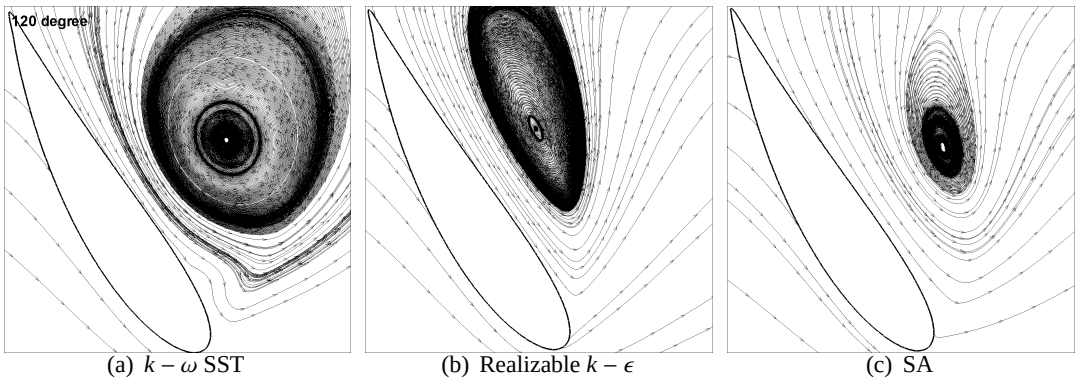

(a) $k - \omega$ SST (b) Realizable $k - \epsilon$ (c) SA

Figure 2.25: Streamlines at 120° for $\lambda = 1.5$

2.2 Comparison with Experimental Results

Two dimensional numerical simulation is performed for all tip speed ratio values, namely $\lambda = 1$, $\lambda = 1.5$, $\lambda = 2$, $\lambda = 2.5$ and $\lambda = 3$, as outlined in Section 2.1.1. The 2D numerical solutions obtained by using $k - \omega$ SST turbulence model are compared with the experimental results as shown in Figures 2.26 through 2.30.

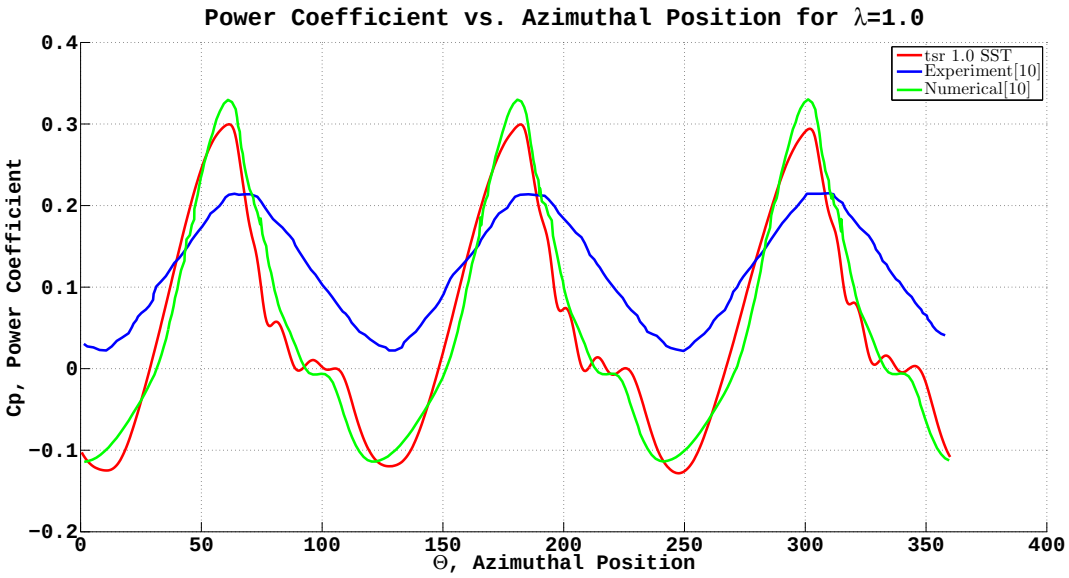

Figure 2.26: Comparison with Experimental Results for $\lambda = 1.0$

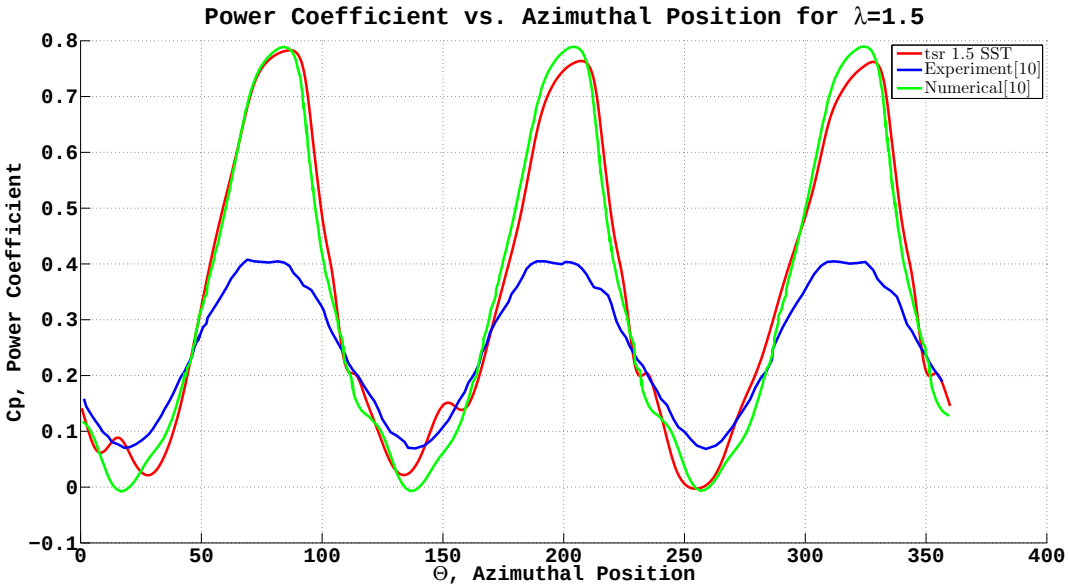

Figure 2.27: Comparison with Experimental Results for $\lambda = 1.5$

Figure 2.26 shows that, the pattern of the numerical and the experimental power coef-

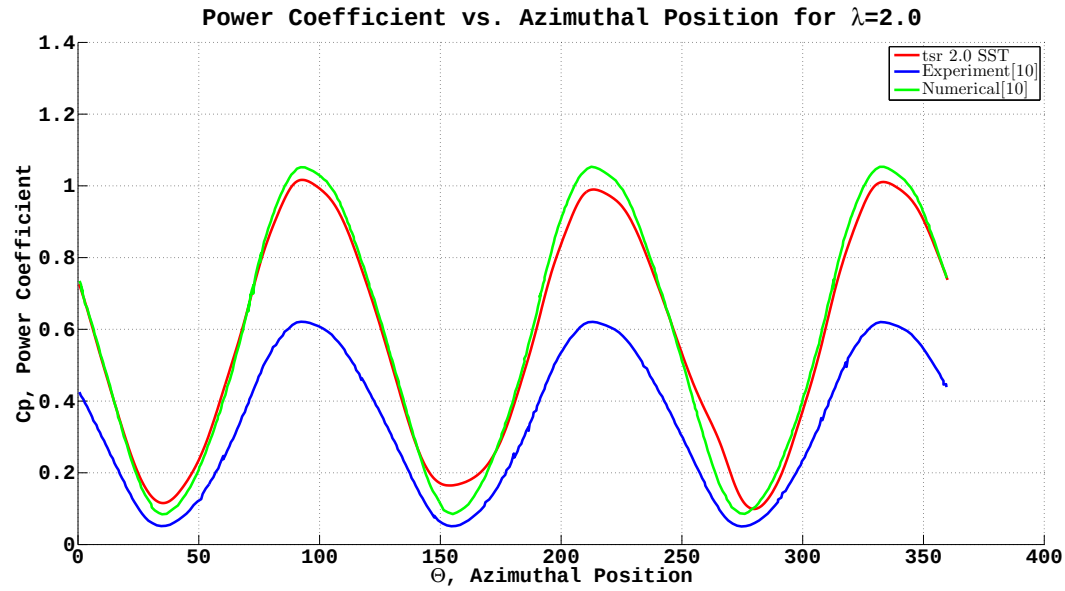

Figure 2.28: Comparison with Experimental Results for $\lambda = 2.0$

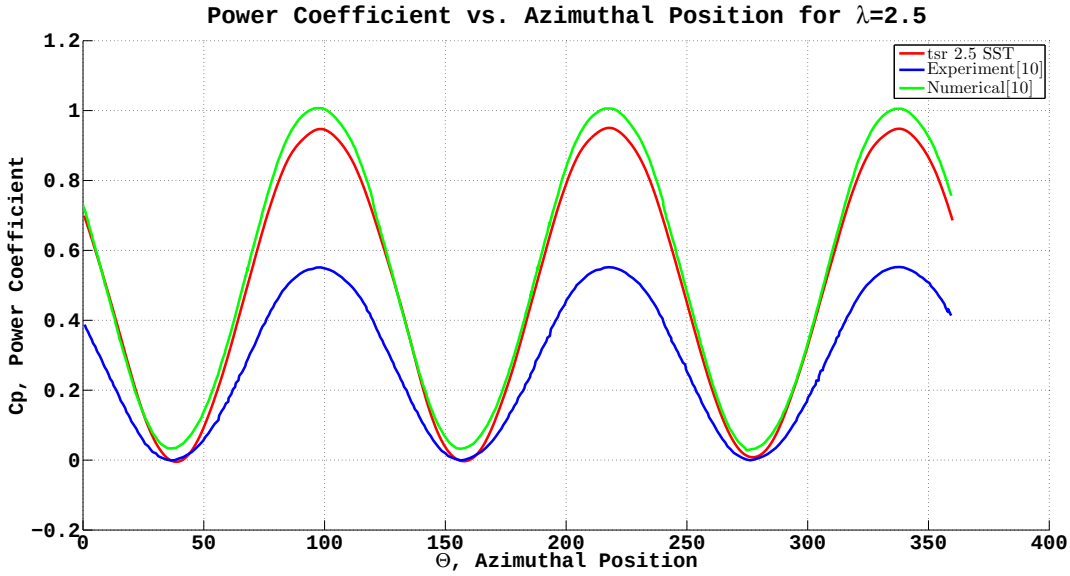

Figure 2.29: Comparison with Experimental Results for $\lambda = 2.5$

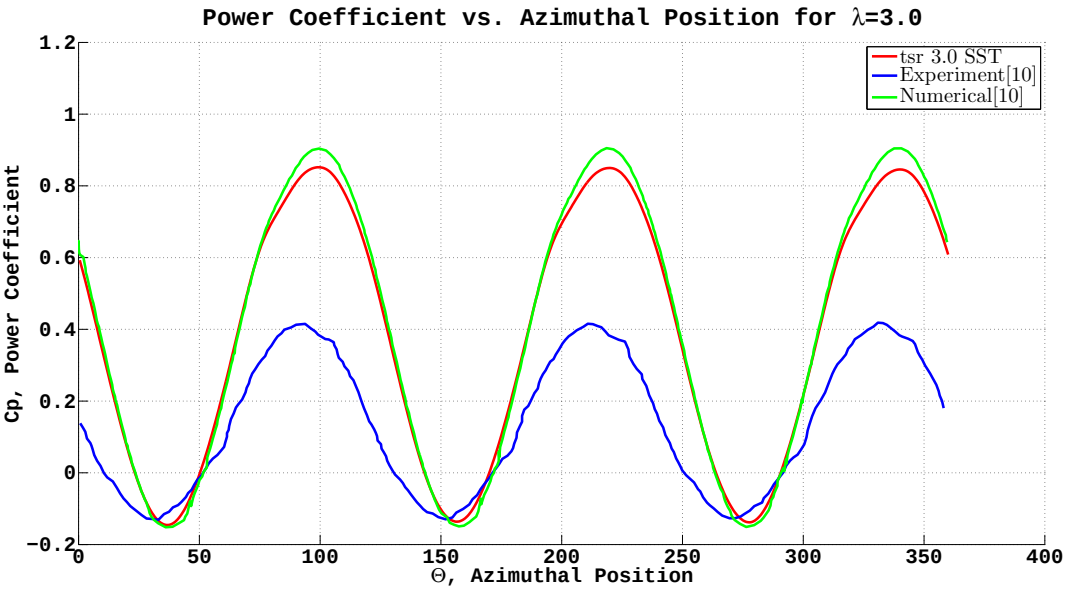

Figure 2.30: Comparison with Experimental Results for $\lambda = 3.0$

ficient curves are quite different for $\lambda = 1.0$. The primary reason might be that flow is very unsteady for $\lambda = 1.0$ and the $k-\omega$ SST model can not predict these unsteady flow conditions. On the other hand, when the Figures 2.27 through 2.30 are analyzed for $\lambda \geq 1.5$, it can be stated that the numerical power coefficient curves show similarity with the experimental power coefficient curves. For these tip speed ratio values, the experimental lower peak values can be estimated by the numerical curve; however, the upper peak values are overestimated.

The comparison between numerical and experimental results for average power coefficients in different tip speed ratio λ values is presented in Figure 2.31. As can be seen in Figure 2.31, For tip speed ratio values, $\lambda \geq 1.5$, the power coefficient values obtained by $k-\omega$ SST turbulence model and experimental data show similar structure. In this region, $k-\omega$ SST turbulence model overestimates the average power coefficients. However, for tip speed ratio value, $\lambda = 1.0$, $k-\omega$ SST turbulence model underestimate the average power coefficient. The reason might be the dynamic stall which is dominant in this region and the flow is very unsteady and contains separations and reattachments.

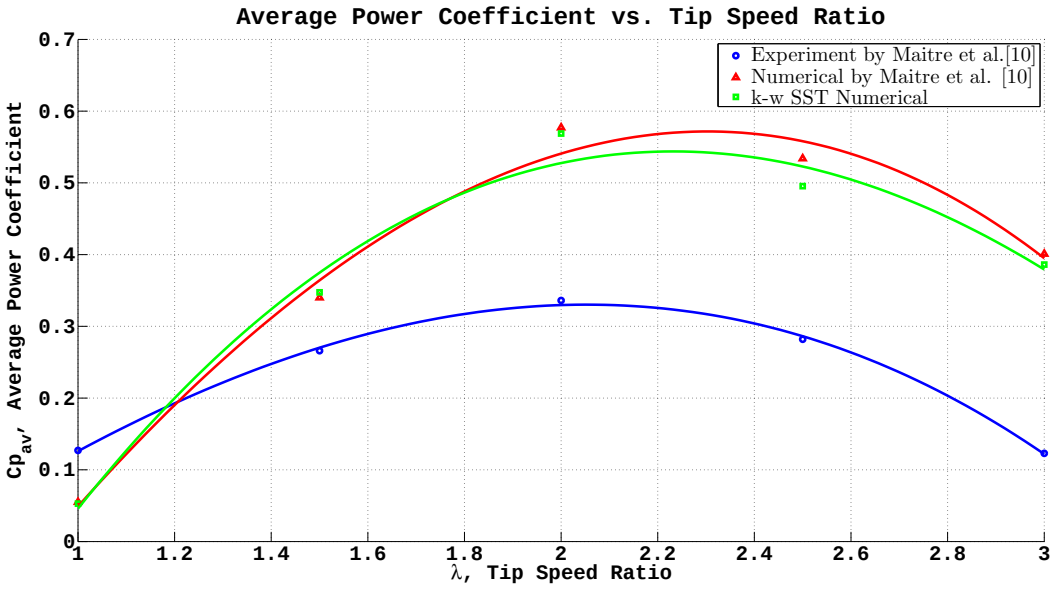

Figure 2.31: Comparison of Numerical and Experimental Results

2.3 Comparison of Turbulence Models

The power coefficients obtained by using different turbulence models are compared for different tip speed ratios. Three different turbulence models, namely, Spalart Allmaras, realizable $k-\epsilon$ with enhanced wall treatment and $k-\omega$ SST turbulence models are used in order to investigate the turbine performance. The results are shown in Figures 2.32 through 2.36.

For $\lambda = 1.0$, the results for Spalart Allmaras and $k-\omega$ SST turbulence models show similarities. Both models underestimate the lower peak values and overestimate the upper peak values when compared with the experimental results. The pattern of the numerical power curves for these two turbulence models are quite different than the the pattern of the experimental curve. On the other hand, the power curve for realizable $k-\epsilon$ turbulence model shows some similarity with the experimental curve. The numerical power curve for $k-\epsilon$ turbulence model converges to the experimental results in the lower peak region; however, it overestimates in the upper peak region as shown in Figure 2.32.

For $\lambda = 1.5$, the results of $k-\omega$ SST and realizable $k-\epsilon$ turbulence models are quite

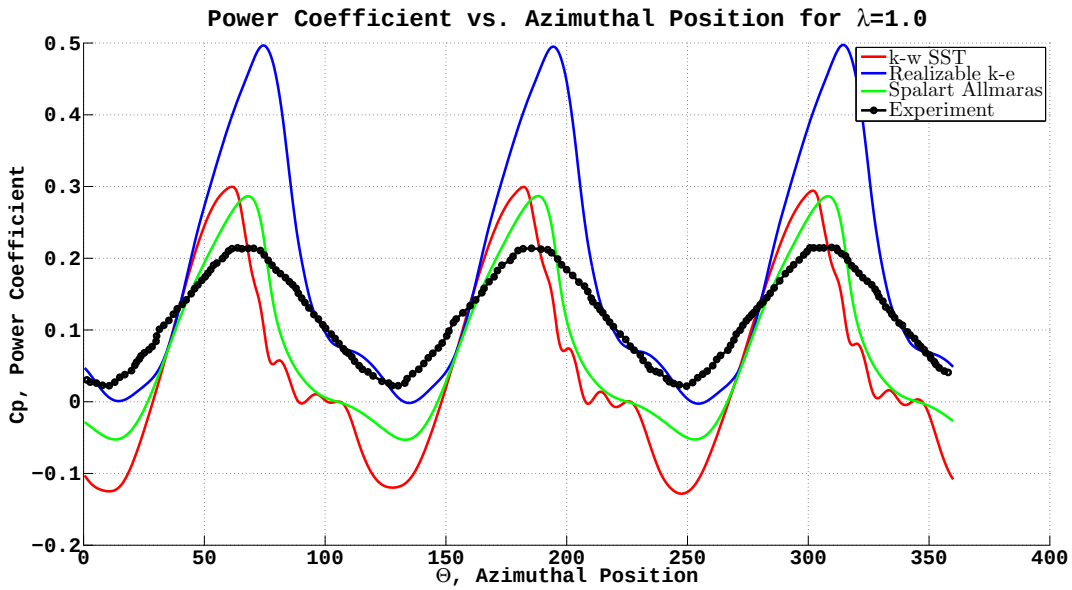

Figure 2.32: Comparison of Turbulence Models for $\lambda = 1.0$

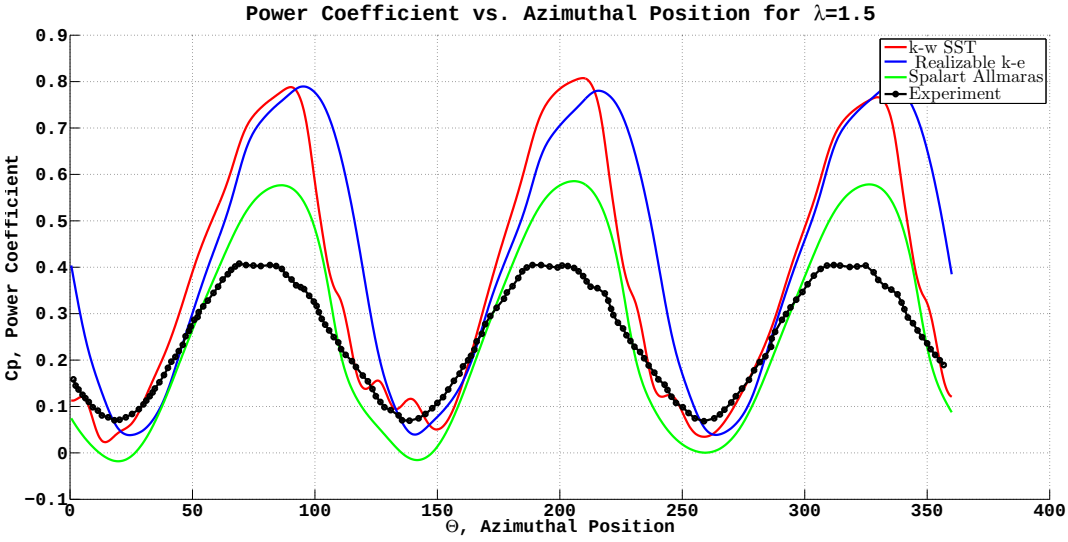

Figure 2.33: Comparison of Turbulence Models for $\lambda = 1.5$

similar. They both converge to the experimental results for the lower peak region and overestimate in the upper peak region. According to the results shown in Figure 2.33, it can be said that the power curve of Spalart Allmaras turbulence model is similar to the experimental power curve although it has some underestimation and overestimation in the lower peak and upper peak regions, respectively.

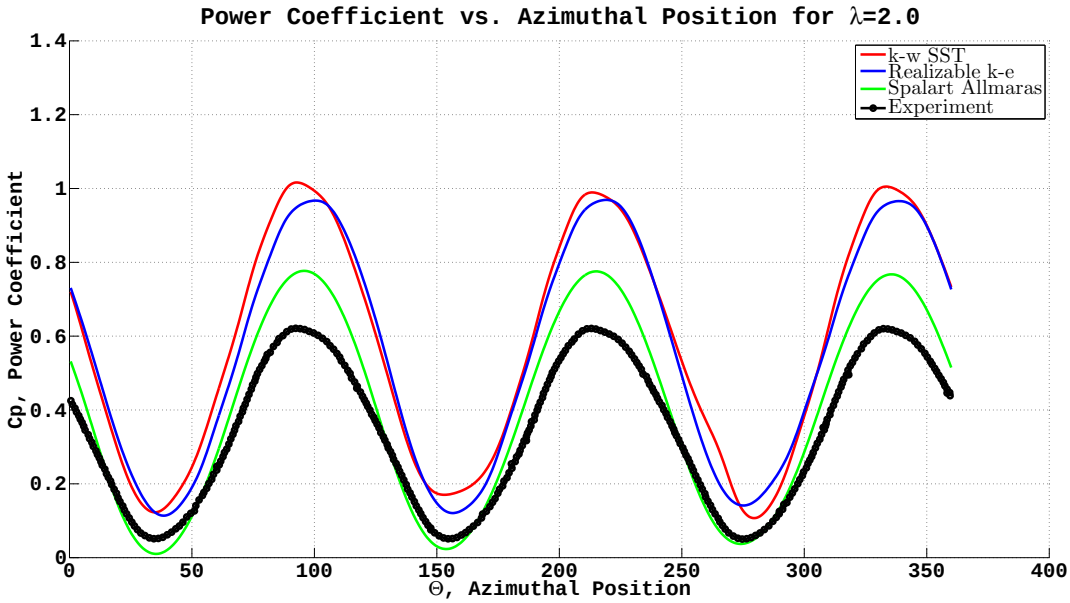

Figure 2.34: Comparison of Turbulence Models for $\lambda = 2.0$

For $\lambda = 2.0$, the results of realizable $k-\epsilon$ and $k-\omega$ SST turbulence models are quite similar. For these turbulence models, it can be said that the results show convergence for the experimental lower peak values; however, the upper peak values are overestimated. The results for Spalart Allmaras turbulence model are quite similar with the experimental results and show some overprediction in the upper peak region as can be seen in Figure 2.34.

For $\lambda = 2.5$, the results of $k-\omega$ SST and realizable $k-\epsilon$ turbulence models are very similar and they converge for the lower peak region and they show overestimation for the upper peak values. As shown in Figure 2.35, it can be said that the power curve of Spalart Allmaras turbulence model is similar to the experimental power curve although it has some underestimation and overestimation in the lower peak and upper peak regions, respectively.

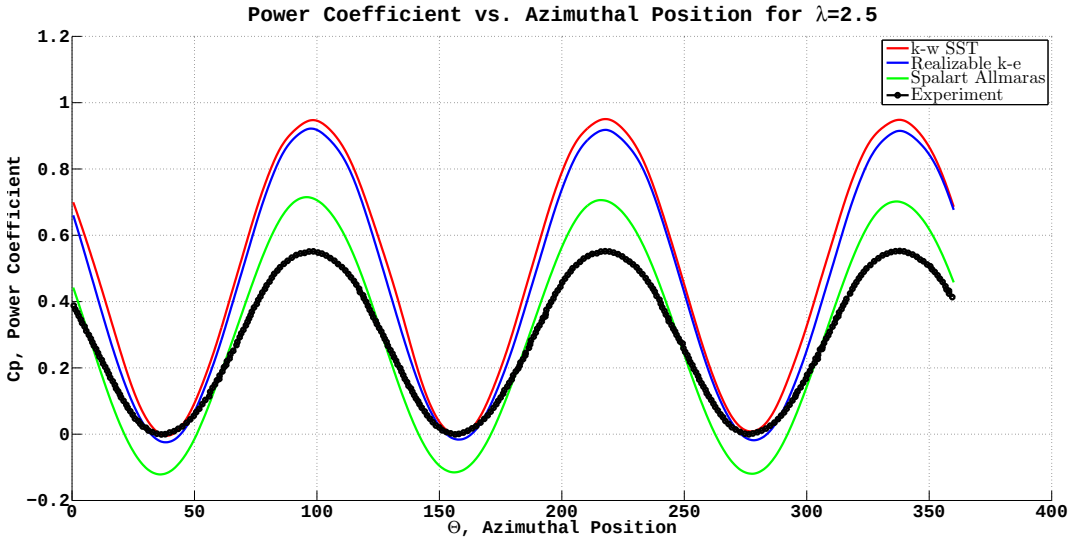

Figure 2.35: Comparison of Turbulence Models for $\lambda = 2.5$

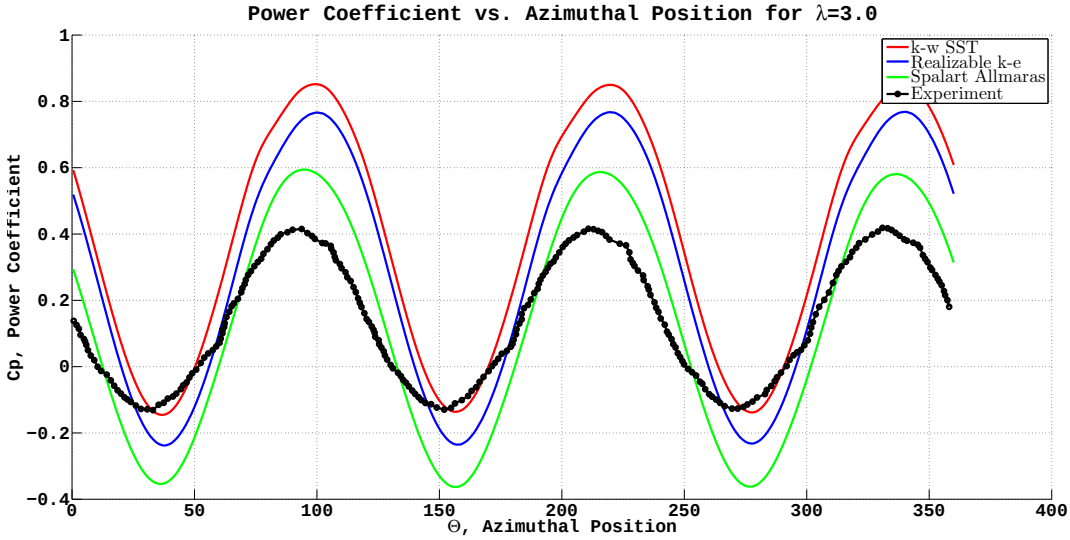

Figure 2.36: Comparison of Turbulence Models for $\lambda = 3.0$

For $\lambda = 3.0$, the results of $k - \omega$ SST and realizable $k - \epsilon$ turbulence models are very similar and they converge for the lower peak region and they show overestimation for the upper peak values. The pattern of the curve for Spalart Allmaras turbulence model is similar with the pattern of the experimental results. However, the results have some overprediction and underestimation as shown in Figure 2.36.

The average power coefficients at different tip speed ratios are shown in Figure 2.37

and compared with the experimental results. Spalart Allmaras and $k-\omega$ SST turbulence models underestimate the average power coefficient for $\lambda = 1$. The primary reason for this can be the dynamic stall which is dominant in the region $\lambda < 1.5$. Realizable $k-\epsilon$ turbulence model results have a constant difference with the experimental results. The reason for this difference might be because of the three dimensional and arm connection losses. Among these three turbulence models, Spalart Allmaras turbulence model shows closest results with the experimental results.

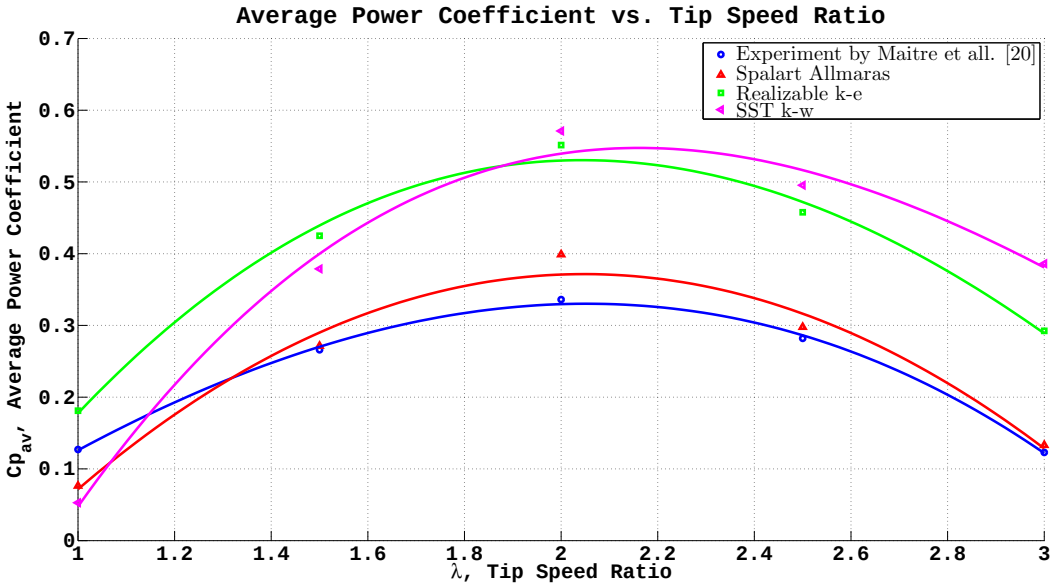

Figure 2.37: Turbulence Model Results for Average Power Coefficient

2.4 Two Dimensional Numerical Solution using Ansys CFX

Another two dimensional numerical study is performed using Ansys CFX commercial sofware which solves Unsteady Navier Stokes equations. 2D calculation domain is the same as the domain mentioned in Section 2.1.2. The interface between rotating and stationary domains are modeled as transient rotor stator model of Ansys CFX which is the equivalent of sliding mesh model of Ansys Fluent. The time step is set to 0.5° rotation of the turbine. The mesh has approximately 266000 elements and it is the same mesh used for the previous numerical studies. SST and SST transition turbulence models are employed for turbulence modeling. The advection scheme and turbulence numerics are set to high resolution and the temporal discretization is set to

second order backward Euler scheme. In addition, residuals are set to $1x10^{-5}$ RMS as convergence criteria. The 2D numerical solutions obtained by using SST and SST transition turbulence models are compared with the experimental results as shown in Figures 2.38 through 2.42.

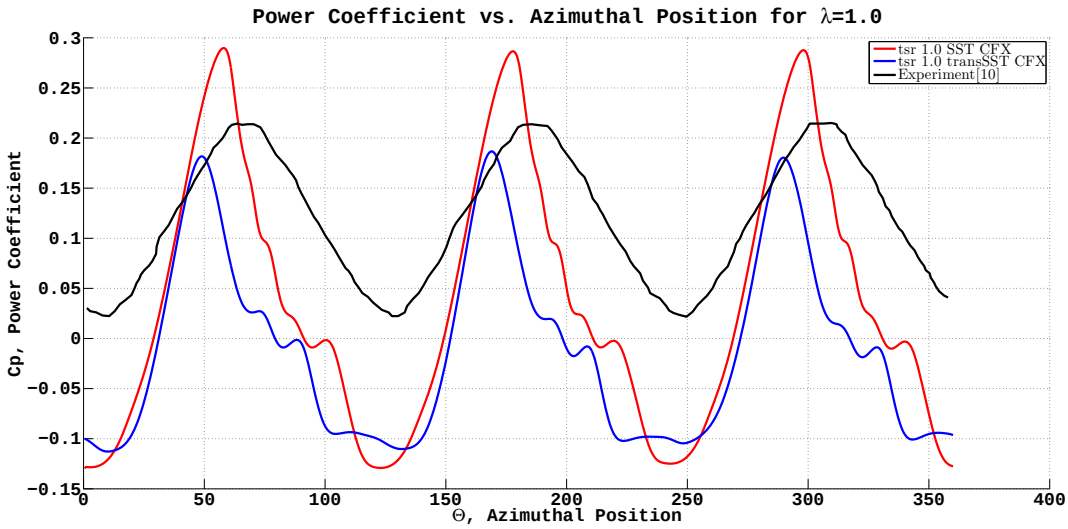

Figure 2.38: Comparison of CFX Turbulence Models Results for λ = 1.0

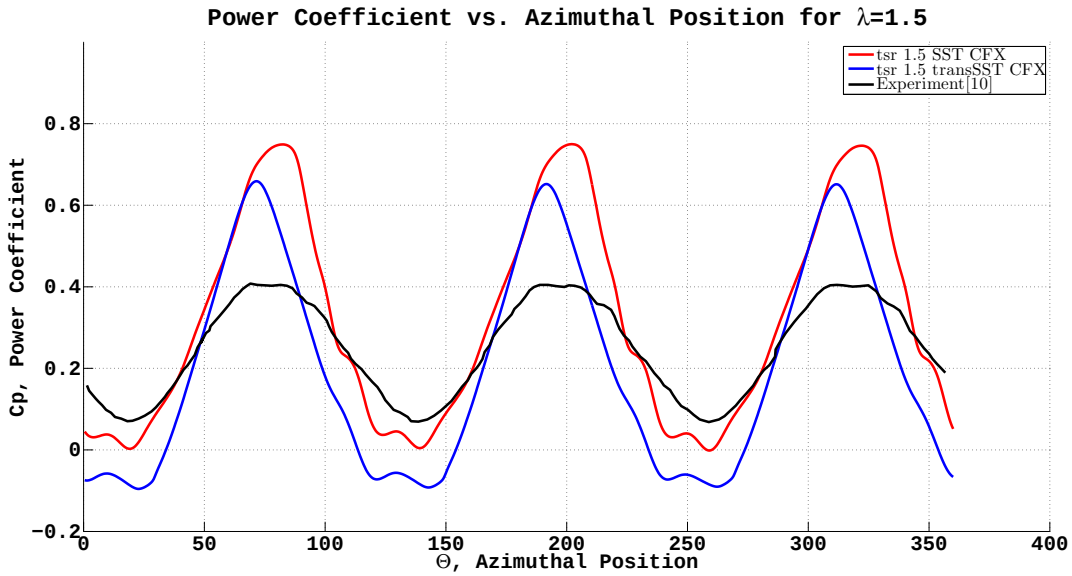

Figure 2.39: Comparison of CFX Turbulence Models for λ = 1.5

The SST and SST transition turbulence model results are almost the same for tip speed ratios of 2.0, 2.5 and 3.0 as shown in Figures 2.40 through 2.42. However, for tip speed ratio values 1.0 and 1.5, they show different results. The reason might be

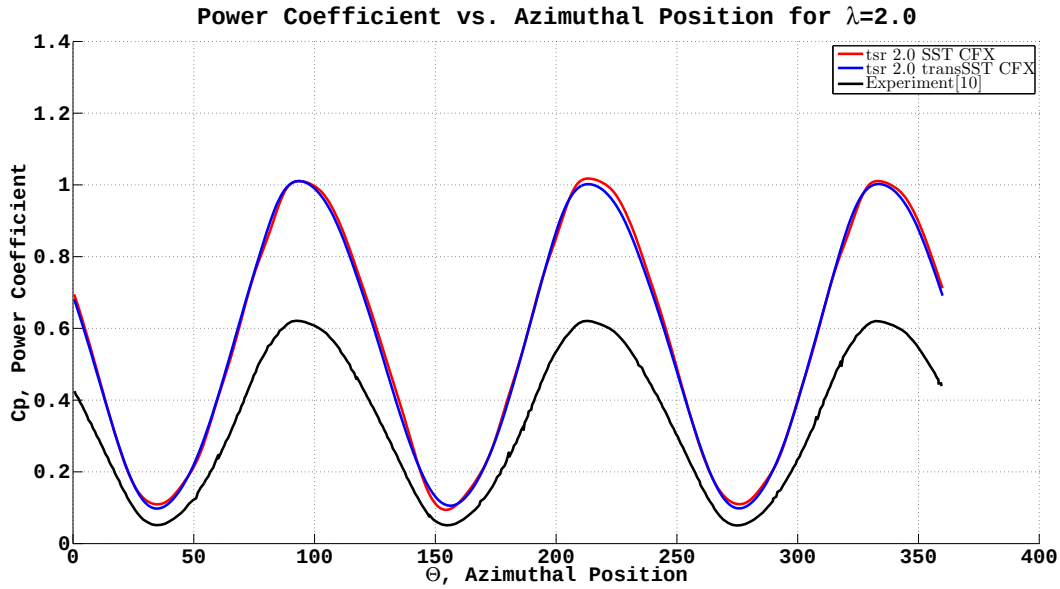

Figure 2.40: Comparison of CFX Turbulence Models for $\lambda = 2.0$

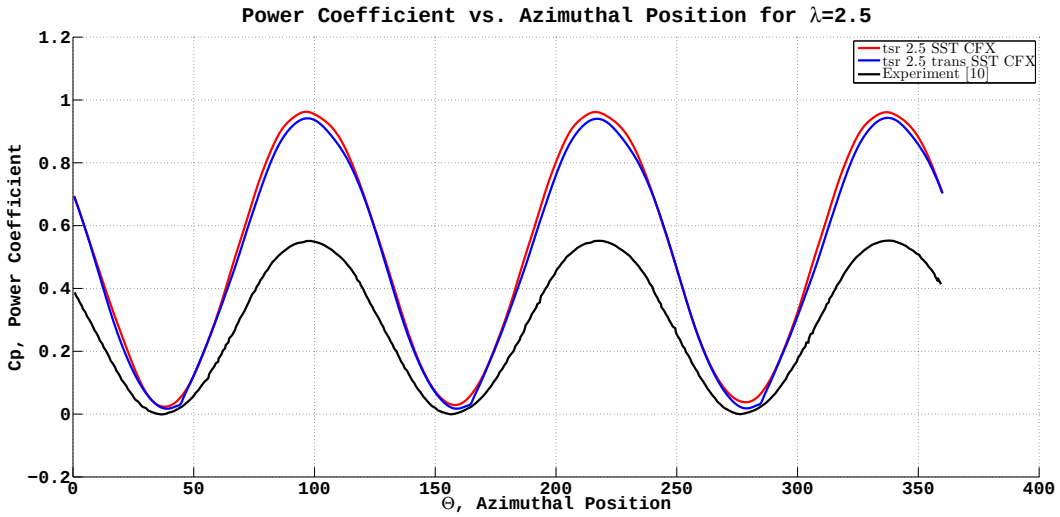

Figure 2.41: Comparison of CFX Turbulence Models for $\lambda = 2.5$

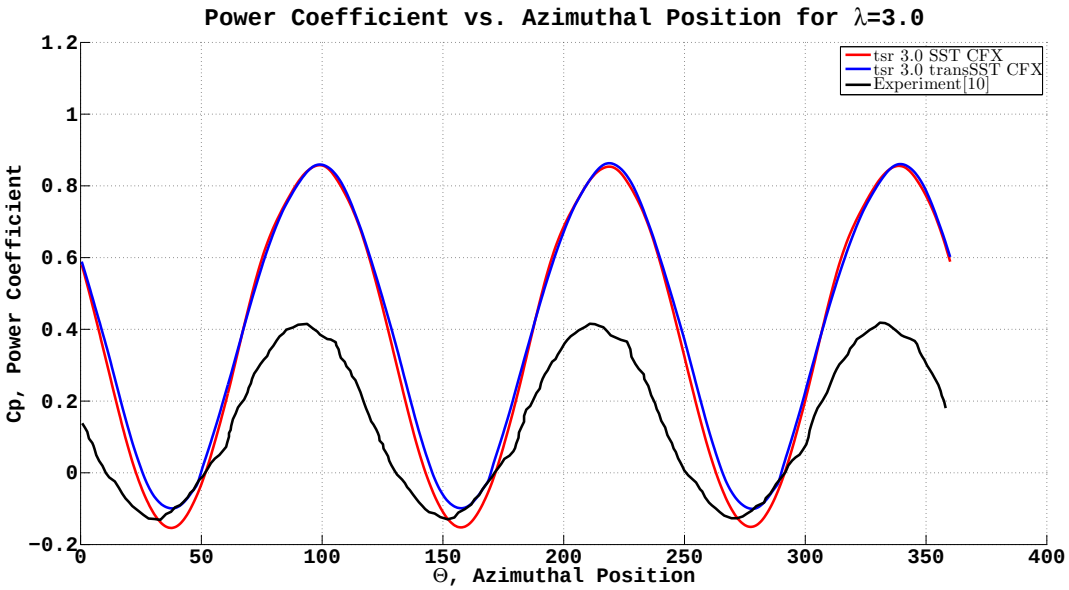

Figure 2.42: Comparison of CFX Turbulence Models for $\lambda = 3.0$

the dominant separations and reattachments for these λ values. In addition, the SST turbulence model results for all tip speed ratios are almost the same as the $k-\omega$ SST results obtained previously by Ansys Fluent. The comparison between numerical and experimental results for average power coefficients in different tip speed ratio λ values is presented in Figure 2.43. The SST transition model predicts lower than SST model for $\lambda = 1.0$ and $\lambda = 1.5$. The average power coefficient obtained by SST transition model is also a negative value for $\lambda = 1.0$. Thus, transition SST model does not perform better than SST turbulence model. Furthermore, the average power coefficients obtained by SST turbulence model of CFX are almost the same with the results of the $k-\omega$ SST turbulence model of Fluent. It is also worth mentioning that the computational cost of using CFX is twice that of Fluent.

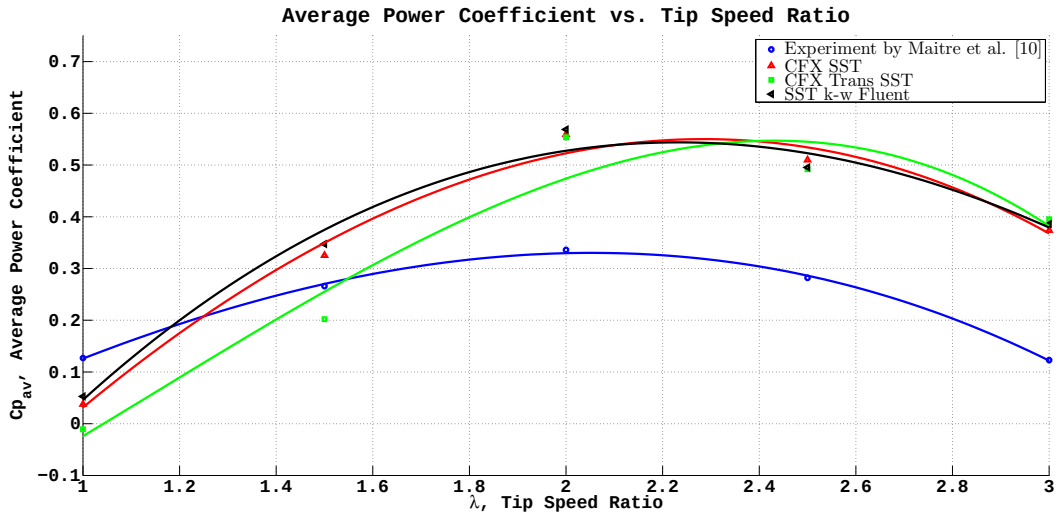

Figure 2.43: CFX Turbulence Model Results for Average Power Coefficient

CHAPTER 3

DESIGN OF A LOW SPEED DARRIEUS TURBINE

Design of the low speed Darrieus turbine for river applications is performed by QBlade. QBlade sofware is developed by the Wind Energy Group at Berlin Technical University Department of Experimental Fluid Mechanics, led by Prof. Dr. Christian Oliver Paschereit. QBlade is a turbine performance calculation software integrated into the airfoil design and analysis program XFOIL. QBlade is used for designing both Horizontal Axis and Vertical Axis Wind/ Water Turbines. QBlade has two sub-modules. One of the sub-modules is HAWT design which is based on Blade Element Momentum (BEM) theory. The other one is VAWT design which is based on Double - Multiple Streamtube Model introduced by Ion Paraschivoiu [14]. In XFOIL, the user can easily design airfoils, compute the polars and extrapolate the polar data to 360° range and integrate them into the design submodules. The design procedure includes,

- Design of airfoil using XFOIL.
- Computation of polar data and extrapolation of the data to 360° angle of attack.
- Design of the turbine rotor using the airfoil created.
- Turbine performance calculation over tip speed ratio λ range based on extrapolated data [34].

The general dimensions of the turbine that is designed is selected to be 700 mm in diameter and 700 mm in height which will be operating in a river current having a speed of 0.4 m/s.

3.1 Selection of the Airfoil

The selection of the airfoil is based on the commonly used airfoils in Darrieus rotors. The airfoils selected for comparison are NACA 0018, NACA 0020 and NACA 0021. The performance analysis of these three airfoils is carried out by assuming that the solidity ratio σ is equal to 1, which is a typical value for Darrieus rotor type water turbines. It is also assumed that the turbine has 3 blades. Based on these assumptions, the chord length of the airfoils is 116.67 mm. The average power coefficients at different tip speed ratio values for different airfoil profiles are shown in Figure 3.1. The average power coefficients for these three profiles are very equal to each other

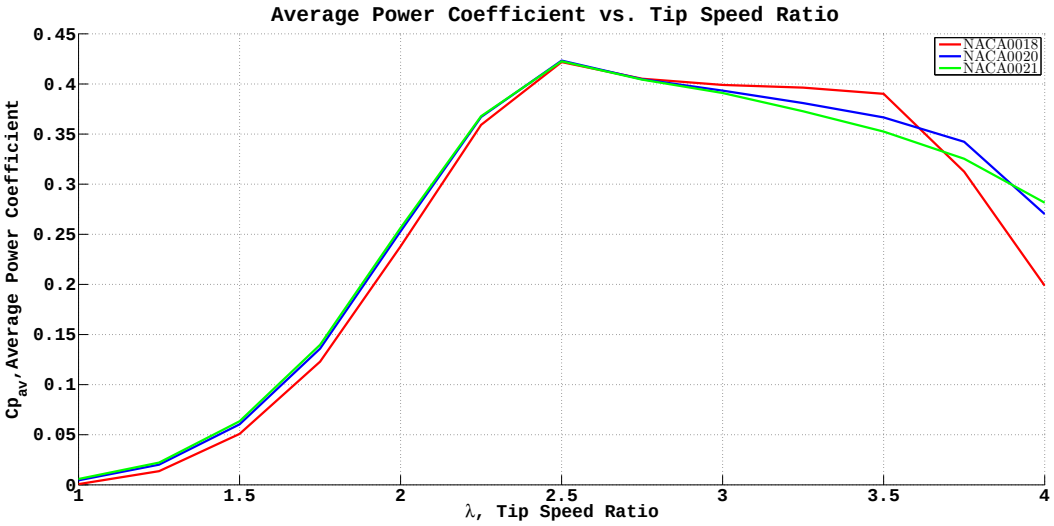

Figure 3.1: Average Power Coefficients for Different Airfoils

as shown in 3.1. NACA 0021 airfoil profile is selected for further design and optimization studies since it has higher average power coefficients for low tip speed ratio values.

3.2 Optimum Solidity Ratio

In order to find the optimum solidity ratio for the selected NACA 0021 airfoil profile, the performance calculations are performed over a range of solidity ratios. The solidity ratios investigated and corresponding blade chord lenghts, *c*, are given in Table 3.1.

Table 3.1: Solidity Ratios and Corresponding Chord Lengths

Solidity ratio, σ	Blade Chord Length, c (mm)
0.8	93.33
1.0	116.67
1.2	140

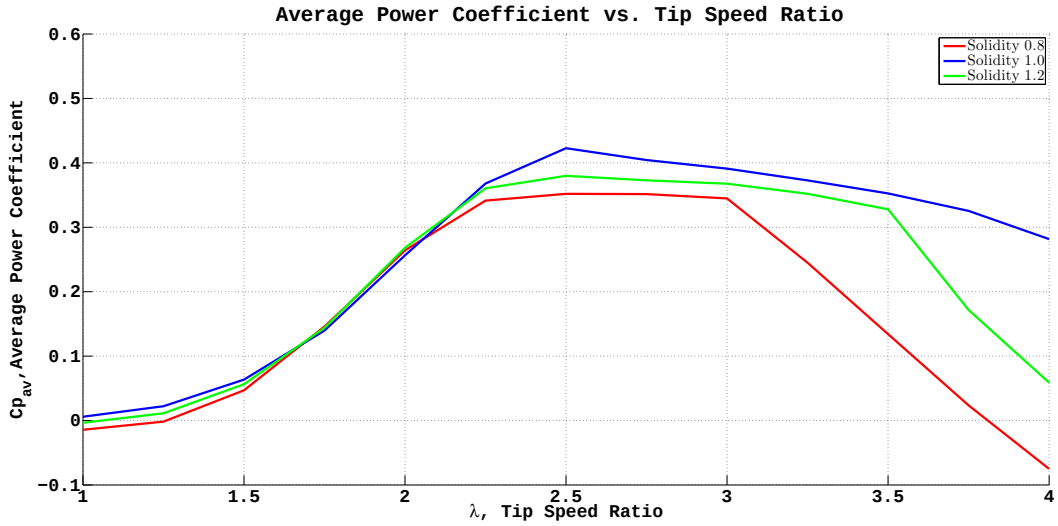

Figure 3.2: Average Power Coefficients for Different Solidity Ratios

The average power coefficient results for different solidity ratios are shown in Figure 3.2. As can be seen in Figure 3.2, σ value 1.0 has highest power coefficient at optimum tip speed ratio when compared with σ values 0.8 and 1.2. Thus, optimum solidity ratio is determined to be 1.0.

3.3 Effect of Camber on Turbine Performance

In the notation of NACA 4 digit airfoils, the first two integers represent the camber line while the last two integers express the thickness of the airfoil. First digit defines the maximum ordinate of camber and second digit defines the location of maximum camber. For example, NACA 2412 airfoil profile means 2 % camber at 40 % chord and 12 % thickness. In order to investigate the effect of camber on the performance, cambers at 20 %, 40 % and 50 % of the chord are analyzed. The average power coefficients change with tip speed ratio values are given in Figure 3.3, Figure 3.4 and Figure 3.5 for 20 %, 40 % and 50 % of the chord, respectively. In these figures, the

performance of cambered airfoils are compared with the base airfoil, NACA 0021.

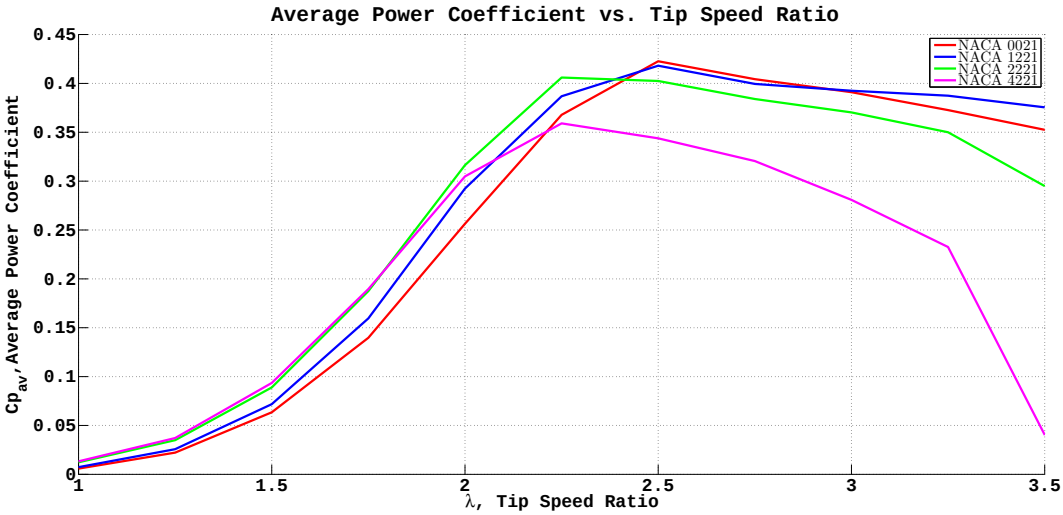

Figure 3.3: Average Power Coefficients for Cambers at 20 % of the chord

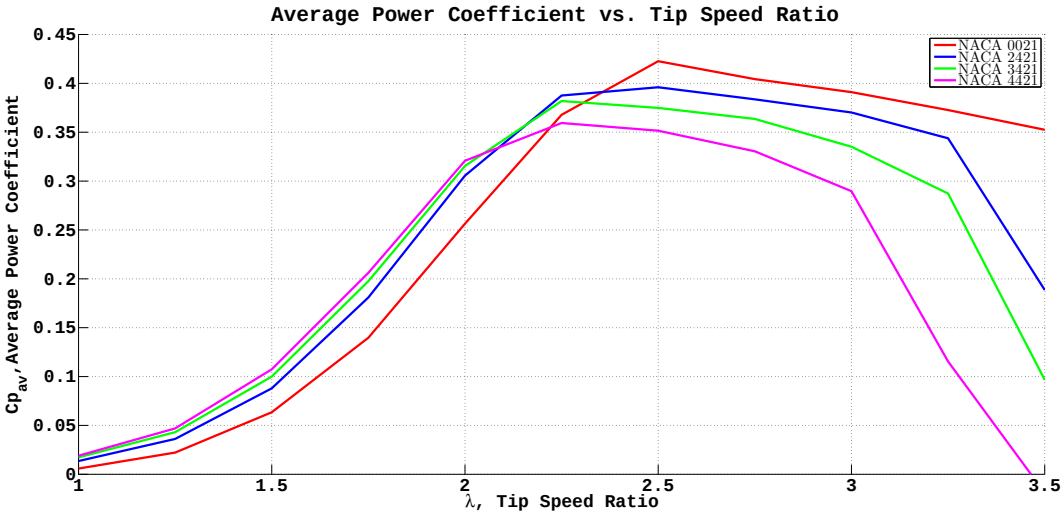

Figure 3.4: Average Power Coefficients for Cambers at 40 % of the chord

As can be seen from the results given in Figures 3.3 through 3.5, although cambered airfoils show improvements on the start up characteristics of the turbine, they do not improve the maximum average power coefficient results. Thus, the base airfoil profile NACA 0021 is kept for further study.

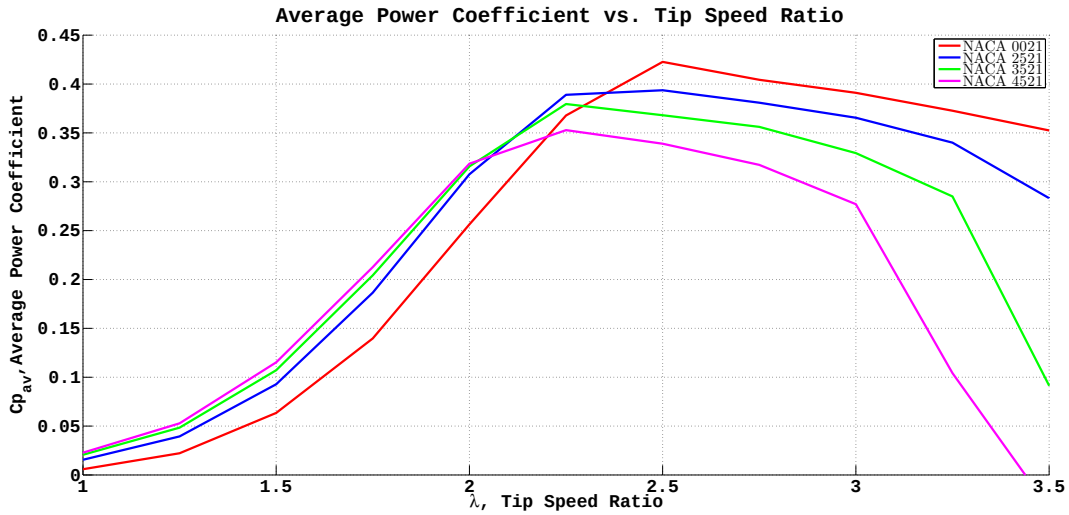

Figure 3.5: Average Power Coefficients for Cambers at 50 % of the chord

3.4 Effect of Maximum Thickness Location

The maximum thickness of the base airfoil NACA 0021 is located at 29.10 % of the chord. In order to examine the effect of the maximum thickness location on the performance, the maximum thickness is changed to the positions % 26.6, % 24.2 and % 19.2 of the chord. The comparison of the average power coefficients for different maximum thickness locations is given in Figure 3.6. The results show that changing

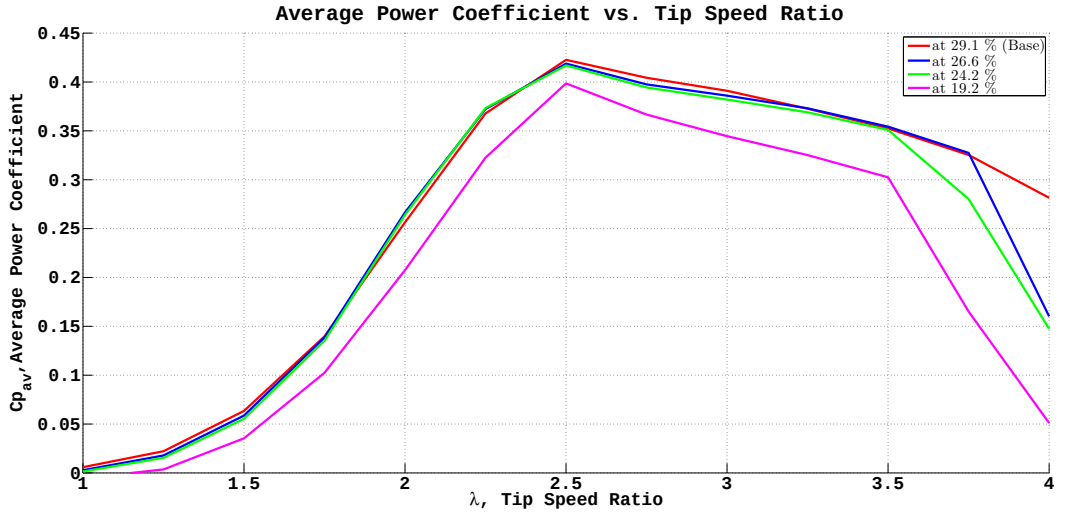

Figure 3.6: Average Power Coefficients for Maximum Thickness Locations

the maximum thickness location of the airfoil does not improve the power coefficient results. Hence, the base airfoil profile NACA 0021 is selected to be the airfoil of the

turbine.

Thus, the final design is decided to be a three bladed turbine with NACA 0021 airfoil profile whose maximum thickness is located at % 29.1 of the chord which is the original position for maximum thickness.

3.5 Two Dimensional Computational Modeling of the Turbine

Two dimensional numerical modeling of the designed turbine is performed by Ansys Fluent using $k - \omega$ SST turbulence model and the average power coefficient results obtained from CFD and QBlade are given in Figure 3.7.

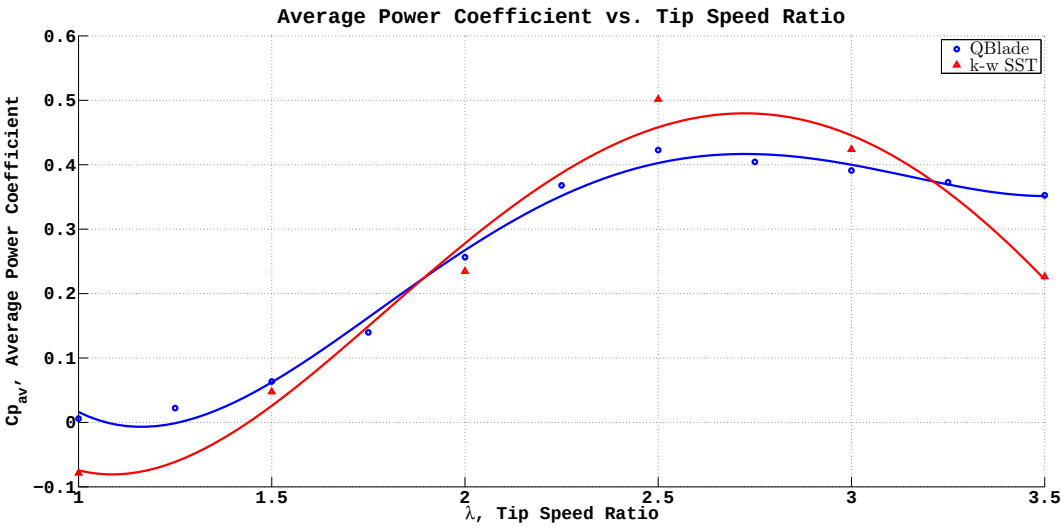

Figure 3.7: Average Power Coefficient Results for CFD and QBlade

Figure 3.7 shows that the average power coefficients obtained by QBlade software is close to the two dimensional numerical results. Thus, it can be said that QBlade is a good tool in order to investigate the performance of vertical axis turbines. However, the results should be compared with experimental results in order to fully evaluate the performance prediction ability of the software.

CHAPTER 4

CONCLUSION

The main aim of this thesis study is to design a Darrieus rotor type vertical axis water turbine to be used in river currents and evaluate its performance by using Computational Fluid Dynamics. Due to the complex flow fields around the blades at different azimuthal positions of the turbine, the numerical modeling of the turbine operation is very important. An experimental Darrieus rotor type vertical axis turbine is selected from literature [10] for two dimensional numerical solution in order to investigate the independent parameters for modeling. Firstly, the independent parameters are investigated including the time step independency, residual independency and mesh independency. This study is concluded by determination of independent time step size, residual set and number of elements in the problem domain based on modeling of this three bladed turbine at the selected tip speed ratio, $\lambda = 1.5$, using commercial CFD package Ansys Fluent.

Secondly, flow field of the selected tip speed ratio, $\lambda = 1.5$, is examined using $k - \omega$ SST, realizable $k - \epsilon$ with enhanced wall treatment and Spallart Almaras turbulence models. The power coefficient change with azimuthal position for the first blade is presented for all turbulence models and the comparison of the performance of the models are done based on the obtained results of vorticity field and streamline. The power curves of different turbulence models have been associated with the related flow fields.

Thirdly, two-dimensional numerical simulation is performed for tip speed ratios, $\lambda = 1.0$ to $\lambda = 3.0$ with increments of 0.5, using three different turbulence mod-

els, namely $k-\omega$ SST, realizable $k-\epsilon$ with enhanced wall treatment and Spallart Almaras turbulence models. The power coefficient results of the turbulence models are compared with the experimental data available.

Next, two dimensional numerical simulation is performed using commercial CFD package ANSYS CFX using SST and SST transition turbulence models. The results obtained by CFX solver are compared with the experimental results.

Finally, a low speed Darrieus type vertical axis water turbine is designed for river applications using QBlade which is an open source software which is used for calculation of the turbine performance based on double multiple streamtube model. Selection of the airfoil profile, determination of the optimum solidity ratio, camber of the airfoil and maximum thickness location are performed. Then, two dimensional numerical modeling of the designed turbine is performed and compared with the results obtained by QBlade.

According to the studies mentioned above, the following conclusions can be done;

- The mesh independency study constitutes one of the most important part of two dimensional computational modeling, since selection of first cell height in the boundary layer mesh of the airfoils plays an important role determining the forces on the blade. On the other hand, determination of independent time step and residual are trivial.
- The main power production occurs between 0° and 150° azimuthal positions for the first blade then the second blade repeats the motion of the first blade and the power production is concluded with the same motion of the third blade for one rotation of the turbine.
- The power coefficient obtained might be related with the width of vorticity in the pressure side of the blade between 0° and 90° azimuthal positions and and this situation may be expressed as the width of vorticity in the pressure side of the first blade increases, the power coefficient obtained becomes smaller.
- The vortex shedding around the shaft is well modeled by $k-\omega$ SST and Spalart

Allmaras turbulence models; however, the vortex shedding is not captured well by $k-\epsilon$ turbulence model.

- The shift of the power coefficient curve for $k-\epsilon$ turbulence model to the right might be related with its late separation estimation.

- The sharp drop in the power coefficient curve for $k-\omega$ SST model after 90° azimuthal position might be related to the size of the separation bubble predicted.

- Spalart Allmaras and $k-\omega$ SST turbulence models underestimate the average power coefficient for $\lambda = 1$. The primary reason for this can be the dynamic stall is which dominant in the region $\lambda < 1.5$. Realizable $k-\epsilon$ turbulence model results have a constant difference with the experimental results. The reason for this difference might be because of the three dimensional effects and arm connection losses. Among these three turbulence models, Spalart Allmaras turbulence model shows closest results with the experimental results.

- SST turbulence model of Ansys CFX gives approximately the same results as the $k-\omega$ SST turbulence model of Ansys Fluent and the transition SST model does not perform better than SST turbulence model.

- The computational cost of using CFX is twice that of Fluent.

- QBlade is a quick tool in order to analyze the performance of vertical axis turbines and the results obtained from QBlade are consistent with CFD results.

Based on the conclusions mentioned above, the following recommendations can be made for 2D CFD modeling of Darrieus turbines in terms of the issues of problem domain, meshing and numerical modeling.

- In order the numerical solution to be independent of problem domain, It is important to determine sizes of the domain. It is recommended that the distance between the inlet boundary condition and the turbine should be five times the diameter of the turbine and the pressure outlet boundary condition should be placed ten times the diameter of the turbine. In addition, the diameters of the rotating domain should be far enough from the blades of the turbine.

- Meshing of the domain constitutes first major part of CFD modeling. In order obtain mesh independent solution, a mesh having a number of elements around 270000 is fine enough. The number of elements in the rotating part should form a large part of this number since the interaction of the blades plays an important role on power production. In addition, the airfoil surfaces should be divided into sufficient number of nodes around 500 which should be denser in the leading and trailing edges of the airfoils in order the separations to be predicted correctly. The determination of the first cell height in the boundary layer mesh of the airfoils is also important since the forces on the blades constitute the power generation. The first cell height should be determined based on chord Reynolds number.

- Numerical modeling is the second major part of CFD modeling. In this study, several turbulence models of Ansys Fluent and CFX are used for numerical solution. It is recommended to use Spalart Allmaras turbulence model for numerical solution since it shows significant similarity with the experimental power coefficient curves. It is also recommended to use Ansys Fluent instead of CFX because the computational cost of using CFX is higher than Fluent, although they give approximately the same results.

As a future work, the designed turbine for low speed river current will be tested in circulating water channel in Department of Mechanical Engineering, METU. 2:1 ratio model will be studied experimentally as a part of a project funded by Coordination of Scientific Research Projects, METU. In addition to the planned future work, the performance of different turbulence models should be compared using PIV data of an experimental Darrieus type vertical axis turbine. Some other turbulence models should also be tested and compared with PIV data in terms of the power coefficient. Three-dimensional numerical modeling should also be performed and compared with the experimental and two-dimensional numerical results. In addition, the experimental power curve of an experimental Darrieus turbine should be compared with the QBlade results in order to fully evaluate QBlade software.

REFERENCES

[1] G. W. Rawlings, "*Parametric Characterization of an Experimental Vertical Axis Hydro Turbine*," M.Sc. Thesis, The University of British Columbia, 2008.

[2] Y. M. Dai and W. Lam, "Numerical Study of Straight-bladed Darrieus-type Tidal Turbine," *ICE - Energy*, vol. 162, no. 2, pp. 67–76, 2009.

[3] I. S. Hwang, Y. H. Lee and S. J. Kim, "Optimization of Cycloidal Water Turbine and the Performance Improvement by Individual Blade Control," *Applied Energy*, vol. 86, no. 9, pp. 1532 – 1540, 2009.

[4] M. Khan, G. Bhuyan, M. Iqbal and J. Quaicoe, "Hydrokinetic Energy Conversion Systems and Assessment of Horizontal and Vertical Axis Turbines for River and Tidal Applications: A Technology Status Review," *Applied Energy*, vol. 86, no. 10, pp. 1823 – 1835, 2009.

[5] M. Mohamed, "Performance Investigation of H-Rotor Darrieus Turbine with New Airfoil Shapes," *Energy*, vol. 47, no. 1, pp. 522 – 530, 2012.

[6] M. Alidadi, "*Duct Optimization for a Ducted Vertical Axis Hydro Current Turbine*," PhD Thesis, The University of British Columbia, 2009.

[7] T. J. Hall, "*Numerical Simulation of a Cross Flow Marine Hydrokinetic Turbine*," M.Sc. Thesis, University of Washington, 2012.

[8] S. Wang, D. B. Ingham, L. Ma, M. Pourkashanian and Z. Tao, "Numerical Investigations on Dynamic Stall of Low Reynolds Number Flow around Oscillating Airfoils," *Computers & Fluids*, vol. 39, no. 9, pp. 1529 – 1541, 2010.

[9] A. Laneville and P. Vittecog, "Dynamic stall: the Case of the Vertical Axis Wind Turbine," *J. Sol. Energy Eng.*, no. May 1986, pp. 6–11, 1986.

[10] T. Maître, E. Amet and C. Pellone, "Modeling of the Flow in a Darrieus Water Turbine: Wall Grid Refinement Analysis and Comparison with Experiments," *Renewable Energy*, vol. 51, pp. 497 – 512, 2013.

[11] M. Islam, D. S.-K. Ting and A. Fartaj, "Aerodynamic Models for Darrieus-type Straight-bladed Vertical Axis Wind Turbines," *Renewable and Sustainable Energy Reviews*, vol. 12, no. 4, pp. 1087 – 1109, 2008.

[12] R. Templin, "*Aerodynamic Performance Theory for the NRC Vertical-axis Wind Turbine*," Tech. Rep., National Aeronautical Establishment, Ottawa (Ontario), 1974.

[13] R. E. Wilson and P. B. Lissaman, "*Applied Aerodynamics of Wind Power Machines*," Tech. Rep., Oregon State University, Corvallis (USA), 1974.

[14] I. Paraschivoiu, "Double-Multiple Streamtube Model for Studying Vertical-Axis Wind Turbines," *Journal of Propulsion Power*, vol. 4, pp. 370–377, Aug. 1988.

[15] H. Hirsh and A. Mandal, "A Cascade Theory for the Aerodynamic Performance of Darrieus Wind Turbines," *Wind Engineering*, 1987.

[16] S. Lain and C. Osorio, "Simulation and Evaluation of a Straight-Bladed Darrieus-type Cross Flow Marine Turbine," *Journal of Scientific and Industrial Research (JSIR)*,vol. 69, no. 12, pp. 906 – 912, 2010.

[17] Y. Li and S. M. Calisal, "Three-Dimensional Effects and Arm Effects on Modeling a Vertical Axis Tidal Current Turbine," *Renewable Energy*, vol. 35, no. 10, pp. 2325 – 2334, 2010.

[18] Y. Nabavi, "*Numerical Study of the Duct Shape Effect on the Performance of a Ducted Vertical Axis Tidal Turbine*," M.Sc. Thesis, The University of British Columbia, 2008.

[19] A. Malipeddi and D. Chatterjee, "Influence of Duct Geometry on the Performance of Darrieus Hydroturbine," *Renewable Energy*, vol. 43, pp. 292 – 300, 2012.

[20] G. Gretton, T. Bruce and D. Ingram, "Hydrodynamic Modelling of a Vertical Axis Tidal Current Turbine using CFD," *Proceedings of the 8th European Wave and Tidal Energy Conference*, pp. 468–476, 2009.

[21] K. Almohammadi, D. Ingham, L. Ma and M. Pourkashan, "Computational Fluid Dynamics (CFD) Mesh Independency Techniques for a Straight Blade Vertical Axis Wind Turbine," *Energy*, vol. 58, pp. 483–493, 2013.

[22] K. M. Almohammadi, D. Ingham, L. Ma and M. Pourkashanian, "CFD Sensitivity Analysis of a Straight-Blade Vertical Axis Wind Turbine," *Wind Engineering*, vol. 36, no. 5, pp. 571–588, 2012.

[23] Y. Kyozuko, "An Experimental Study on the Darrieus-Savonius Turbine for the Tidal Current Power Generation," *Journal of Fluid Science and Technology*, vol. 3, no. 3, pp. 439–449, 2008.

[24] M. Shiono, K. Suzuki and S. Kiho, "An Experimental Study of the Characteristics of a Darrieus Turbine for Tidal Power Generation," *Electrical Engineering in Japan*, vol. 132, no. 3, pp. 38–47, 2000.

[25] R.Nobile, M.Vahdati, J. Barlow and A. Newburn-Crook, "Dynamic Stall for a Vertical Axis Wind Turbine in a Two-dimensional Study," *Proceedings of World Renewable Energy Congress*, 2011.

[26] A. Allet, S. Hallé and I. Paraschivoiu, “Numerical Simulation of Dynamic Stall around an Airfoil in Darrieus Motion,” *Journal of Solar Energy Engineering*, vol. 121, no. 1, pp. 69–76, 1999.

[27] S. Wang, D. B. Ingham, L. Ma, M. Pourkashanian and Z. Tao, “Turbulence Modeling of Deep Dynamic Stall at Relatively low Reynolds Number,” *Journal of Fluids and Structures*, vol. 33, pp. 191 – 209, 2012.

[28] C. S. Ferreira, H. Bijl, G. Van Bussel and G. Van Kuik, “Simulating Dynamic Stall in a 2D VAWT: Modeling Strategy, Verification and Validation with Particle Image Velocimetry Data,” *Journal of Physics: Conference Series*, vol. 75, no. 1, IOP Publishing, 2007.

[29] C. S. Ferreira, G. Van Bussel, F. Scarano and G. van Kuik, “2D PIV Visualization of Dynamic Stall on a Vertical Axis Wind Turbine,” *Proceedings of 45th AIAA Aerospace Sciences Meeting and Exhibit/ASME Wind Energy Symposium*, 2007.

[30] K. W. McLaren, “*A Numerical and Experimental Study of Unsteady Loading of High Solidity Vertical Axis Wind Turbines*,” PhD Thesis, McMaster University, 2011.

[31] J. Tu, G. H. Yeoh and C. Liu, “*Computational Fluid Dynamics: a Practical Approach*,” Butterworth-Heinemann, 2007.

[32] “*Fluent 12.0 Theory Guide*,” Ansys Inc, vol. 5, 2009.

[33] H. Schlichting and J. Kestin, *Boundary-Layer Theory*, vol. 539, McGraw-Hill, New York, 1968.

[34] D. Marten and J. Wendler, “*Qblade Guidelines*,” 2013.